

Full view on the dynamics of an impurity coupled to two one-dimensional bathsMartino Stefanini ¹, Massimo Capone,^{1,2} and Alessandro Silva¹¹*International School for Advanced Studies (SISSA), Via Bonomea 265, 34136 Trieste, Italy*²*CNR-IOM Democritos, Via Bonomea 265, 34136 Trieste, Italy*

(Received 27 September 2022; revised 15 April 2023; accepted 2 May 2023; published 31 May 2023)

We consider a model for the motion of an impurity interacting with two parallel, one-dimensional baths, described as two Tomonaga-Luttinger liquid systems. The impurity is able to move along the baths, and to jump from one to the other. We provide a perturbative expression for the evolution of the system when the impurity is injected in one of the baths, with a given wave packet. We obtain an approximation formally of infinite order in the impurity-bath coupling, which allows us to reproduce the orthogonality catastrophe. We monitor and discuss the dynamics of the impurity and its effect on the baths, in particular for a Gaussian wave packet. Besides the motion of the impurity, we also analyze the dynamics of the bath density and momentum density (i.e., the particle current), and show that it fits an intuitive semiclassical interpretation. We also quantify the correlation that is established between the baths by calculating the interbath, equal-time spatial correlation functions of both bath density and momentum, finding a complex pattern. We show that this pattern contains information on both the impurity motion and on the baths, and that these can be unveiled by taking appropriate “slices” of the time evolution.

DOI: [10.1103/PhysRevB.107.184316](https://doi.org/10.1103/PhysRevB.107.184316)**I. INTRODUCTION**

Impurity problems have been a source of fruitful ideas in condensed matter physics for decades. The most famous one is probably the Kondo effect [1–3], in which a fixed spin interacts with a bath of noninteracting electrons, causing an anomalous resistive behavior at low temperature. While in the Kondo problem the impurity is immobile, a large literature has been devoted to see what happens if the foreign particle can move. The idea traces back at least to Landau [4,5] who introduced the concept of “polaron” in a solid-state framework to describe the quasiparticle arising from a strong coupling of an electron with lattice phonons [2,6].

In the last three decades, the progress of ultracold atom experiments [7–9] offered new possibilities in the study of impurity problems. The experimental flexibility and control over the various parameters has allowed for a precise investigation of both immobile and mobile impurities, such as foreign atoms in Bose-Einstein condensates [10] and in Fermi gases [11]. In particular, a one-dimensional (1D) setting, in which impurities are restricted to move along elongated baths, has revealed some remarkable phenomena, such as Bloch oscillations even in the absence of a lattice [12]. Indeed, the specificity of one spatial dimension has stimulated a large array of theoretical and experimental studies [13,14].

In a recent paper [15], the authors considered a model of a mobile impurity that is able to jump between two bosonized 1D baths. This model was meant to provide a simplified perspective of the dynamics of an excitation (the impurity) in a heterostructure, with the baths playing the role of the “layers”. This investigation was inspired by the budding field of oxide heterostructure engineering [16,17], and in particular by the question of the conditions under which quantum-mechanical coherence can improve transport of the excitation through the

heterostructure [18]. In Ref. [15] the topic was addressed by computing the Green’s function of the impurity.

In the present paper, we propose an improved perturbative treatment that is able to reproduce the Green’s function calculated in [15], while providing the time evolution for the whole system formed by the impurity and the baths. Thus, we can access the time evolution of any observable (while correlation functions at different times are not directly accessible). Moreover, the numerical effort required is modest enough to allow the study of a large subset of the possible initial momentum distributions of the impurity. We will present the time evolution of some observables for a Gaussian wave packet. We will discuss the dynamics of the probability distribution for the impurity, observing how the motion and the spreading of the wave packet is influenced by the baths. We will also take a different perspective on the polaron dynamics, focusing on the effects of the impurity on the baths. Hence, we will show how the density and current in the baths are modified, and how the exchange of the impurity between the baths is reflected in the shape of their density correlations.

The paper is organized as follows: In Sec. II we introduce the model, and prepare the ground for the perturbative treatment by performing a suitable unitary transformation on the Hamiltonian, obtaining a simpler one. We summarize the main results in Sec. III. The following two sections are technical in nature. In Sec. IV we explain the improved perturbative technique that we used to obtain the evolution of the full impurity-bath state. In Sec. V we illustrate the observables that we will focus on in the rest of the paper, and we provide the expressions of their expectation values. Finally, in Sec. VI we present the results of our numerical computations of the various observables. In Sec. VII we sum up our findings and provide some outlook. We have confined some more technical points to the Appendices.

II. DEFINITION OF THE MODEL

In this section we define our model and the main assumptions and approximations behind it. We also employ a widely-known unitary transformation to simplify the Hamiltonian in a form that is more suitable for the perturbative calculation of the dynamics.

We consider a fermionic impurity, which moves along a ladder, which hosts two one-dimensional (1D) interacting baths [19] on its two legs. These baths are independent of each other, and the impurity interacts with each of them. We take the length of the system to be $L = Na$ (a being the lattice spacing), and we work in periodic boundary conditions (pbc). The Hamiltonian is

$$\mathcal{H} = \mathcal{H}_{\text{imp}} + \mathcal{H}_{\text{bath}} + \mathcal{H}_c, \quad (1)$$

where the noninteracting impurity part is

$$\begin{aligned} \mathcal{H}_{\text{imp}} = & 2J_{\parallel} \sum_{j\sigma} d_{j\sigma}^{\dagger} d_{j\sigma} - J_{\parallel} \sum_{j\sigma} (d_{j+1,\sigma}^{\dagger} d_{j\sigma} + \text{H.c.}) \\ & - J_{\perp} \sum_{j\sigma} d_{j\sigma}^{\dagger} d_{j\sigma}. \end{aligned} \quad (2)$$

The index j enumerates the lattice sites along the chains, while the pseudospin $\sigma = \uparrow, \downarrow$ (or equivalently $\sigma = \pm 1$ used in the equations) specifies the chain. We will assume that the interbath hopping J_{\perp} is (much) smaller than the intrabath one J_{\parallel} .

We will often use a momentum space representation for the impurity,

$$d_{j\sigma} = \frac{1}{\sqrt{N}} \sum_p e^{ipaj} d_{p\sigma}, \quad (3)$$

so that

$$\mathcal{H}_{\text{imp}} = \sum_{p\sigma} (E(p) d_{p\sigma}^{\dagger} d_{p\sigma} - J_{\perp} d_{p\sigma}^{\dagger} d_{p\sigma}), \quad (4)$$

where $E(p) = 2J_{\parallel}(1 - \cos(pa))$. In the low-energy limit we will approximate

$$E(p) \simeq \frac{p^2}{2M}, \quad (5)$$

where $M^{-1} = 2J_{\parallel}a^2$. We diagonalize \mathcal{H}_{imp} in terms of even (e) and odd (o) modes

$$d_{p,\mu=e/o} = \frac{1}{\sqrt{2}}(d_{p,1} \pm d_{p,-1}) \quad (6)$$

$$\Rightarrow \mathcal{H}_{\text{imp}} = \sum_{p\mu} \lambda_{p\mu} d_{p\mu}^{\dagger} d_{p\mu}, \quad (7)$$

where $\lambda_{p,e/o} = E(p) \mp J_{\perp}$.

We are interested in the low-energy, long-wavelength behavior, therefore we use bosonization (see [20,21]) to write the bath Hamiltonian as a pair of Tomonaga-Luttinger liquids (TLLs) with sound speeds v_{σ} and Luttinger parameters K_{σ} (encoding the intrabath interactions) [22],

$$\mathcal{H}_{\text{bath}} = \sum_{\sigma} v_{\sigma} \int \frac{dx}{2\pi} \left[K_{\sigma} \left(\frac{d}{dx} \theta_{\sigma}(x) \right)^2 + \frac{1}{K_{\sigma}} \left(\frac{d}{dx} \phi_{\sigma}(x) \right)^2 \right], \quad (8)$$

with $[\phi_{\sigma}(x), \theta_{\sigma'}(y)] = -i\delta_{\sigma,\sigma'} \arg(\alpha + i(x-y))$, α being a small length scale acting as a UV cutoff. For simplicity, we assume that the particles constituting the baths carry no spin. Finally, in the spirit of a low-energy approximation, we use a simple density-density contact interaction,

$$\mathcal{H}_c = \sum_{j\sigma} g_{\sigma} d_{j\sigma}^{\dagger} d_{j\sigma} \rho_{\sigma}(ja), \quad (9)$$

where we take the long-wavelength approximation $\rho_{\sigma}(x) = \bar{\rho}_{\sigma} - 1/\pi d\phi_{\sigma}(x)/dx$ [20]. The first term is the average density. If the baths have identical properties, this term can be discarded because it is only an overall energy shift. This will be the case for all numerical calculations of this paper.

Expressing the bath fields $\phi_{\sigma}(x)$, $\theta_{\sigma}(x)$ in terms of the boson modes $b_{q\sigma}$ that diagonalize $\mathcal{H}_{\text{bath}}$ (we follow the conventions of [20]), we find

$$\mathcal{H}_{\text{bath}} = \sum_{q \neq 0, \sigma} v_{\sigma} |q| b_{q\sigma}^{\dagger} b_{q\sigma}, \quad (10)$$

$$\mathcal{H}_c = \sum_{j\sigma} \sum_{q \neq 0} \frac{W_{q\sigma}}{L^{1/2}} d_{j\sigma}^{\dagger} d_{j\sigma} (e^{-iqaj} b_{q\sigma}^{\dagger} + e^{iqaj} b_{q\sigma}), \quad (11)$$

where we defined

$$W_{q\sigma} \equiv g_{\sigma} K_{\sigma}^{1/2} \frac{|q|^{1/2}}{(2\pi)^{1/2}}. \quad (12)$$

We notice from this equation that the only effect of the interactions acting between the particles constituting the baths is a rescaling of the impurity-bath coupling, according to $g_{\sigma} \rightarrow g_{\sigma} K_{\sigma}^{1/2}$. This rescaling implies that the intrabath interactions can only enhance or reduce the impurity-bath coupling with respect to baths consisting of free particles (which have $K_{\sigma} = 1$). Bosonic baths with short-range interactions (necessarily repulsive) can only realize the former situation ($K_{\sigma} > 1$), whereas fermionic baths can have both $K_{\sigma} < 1$ (repulsive interactions) and $K_{\sigma} > 1$ (attractive interactions) [20]. The rescaling of the impurity-bath coupling is the only effect of intrabath interactions for impurity observables (e.g., the impurity density), while bath observables such as the density and momentum also explicitly depend on K_{σ} . The dependence of the bath observables on the Luttinger parameter K_{σ} and on the coupling g_{σ} is discussed in Secs. [VID](#) and [VIE](#).

A technical remark: The description of the baths as TLLs is an effective field theory, valid up to a momentum (energy) cutoff α^{-1} (Λ). Therefore, we will endow $W_{q\sigma} \rightarrow W_{q\sigma} e^{-\alpha|q|/2}$ with a momentum cutoff whenever we will find divergent expressions.

We will refer to the quasiparticles described by the operators $b_{q\sigma}$ as phonons, as they indeed correspond to quantized density oscillations with an acoustic dispersion relation $\omega_{q\sigma} = v_{\sigma} |q|$ [20].

We add a few remarks on the approximations involved in our effective model. The relation between the microscopic model and the effective one is depicted in Fig. 1, in the main experimental scenario that we have in mind, namely that of fermionic baths. The figure shows the filled Fermi sea of one of the baths (which are assumed to be identical) and the lattice dispersion of the two free impurity bands (continuous lines). The low-energy model, shown as dashed lines, assumes that the dispersion of the baths can be linearized around the

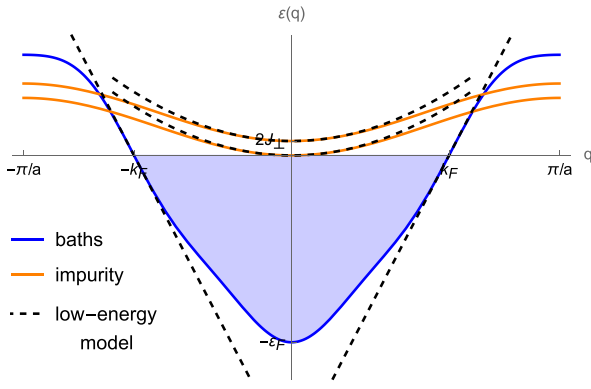


FIG. 1. Qualitative depiction of the band dispersion for one of the baths (blue) and of the impurity (orange) in a generic microscopic theory, and their low-energy approximations in the effective model (dashed lines). The image illustrates the hierarchy of energy and momentum scales in the unperturbed theory (i.e., in absence of impurity-bath coupling). The baths are assumed to be made of fermions, filling the band up to the Fermi energy (colored area). The relative position of the bottom of the impurity and bath bands is irrelevant for the low-energy physics. Indeed, the bath Fermi energy ε_F does not play any role in our treatment.

Fermi points, while that the dispersion of the impurity can be approximated as parabolic (both assumptions correspond to low momentum with respect to the Fermi momentum k_F). Figure 1 also shows the hierarchy of energy scales in our model, with the typical impurity energies (i.e., its momentum and the gap $2J_\perp$) being much smaller than the baths' Fermi energy and width of the region in which the linearization of the dispersion is valid.

In general, the long-wavelength expansion of the bosonized bath density in Eq. (9) should contain terms of the form $\cos[2p(\bar{\rho}_\sigma x - \phi_\sigma(x))]$ [20], with $p = 1, 2, \dots$. These terms describe backscattering of the bath particles off the impurity [12,20,21] with momentum exchange that is multiple of $2\pi\bar{\rho}_\sigma = 2k_{F\sigma}$, where the latter expression applies to a spinless fermionic bath. We have chosen to neglect these backscattering terms in Eq. (9). Our approximation is justified by the fact that we assume that the impurity momentum is much smaller than $2\pi\bar{\rho}_\sigma$. In addition, while the calculations described below in Sec. IV are nonperturbative in J_\perp , since the deexcitation of the odd mode is accompanied by the emission of phonons of energy of about $2J_\perp$, this energy (or, equivalently, the wave number $q \sim 2J_\perp/v_\sigma$) must be small enough so that the bosonized description of the baths in terms of sound modes applies. At the same time $2J_\perp \ll 2k_{F\sigma}v_\sigma$ in order to ensure that we can neglect the above-mentioned cosine term in the bosonized density.

A. The Lee-Low-Pines transformation

The Hamiltonian presented in the previous paragraphs can be cast in a simpler form that we will use in the perturbative calculation. In polaron problems, it has long been known [23] that it is possible to take advantage of the conservation of the total polaron momentum $P_{\text{tot}} = \sum_{p\sigma} p d_{p\sigma}^\dagger d_{p\sigma} + \sum_{q \neq 0, \sigma} q b_{q\sigma}^\dagger b_{q\sigma}$. This is achieved by performing a unitary

transformation, first introduced by Lee, Low, and Pines (LLP),

$$\mathcal{H}_{\text{LLP}} \equiv U_{\text{LLP}}^\dagger \mathcal{H} U_{\text{LLP}}, \quad U_{\text{LLP}} = e^{-iX P_b}, \quad (13)$$

with

$$X = a \sum_{j\sigma} j d_{j\sigma}^\dagger d_{j\sigma} \quad (14)$$

being the impurity position operator [24] and

$$P_b = \sum_{q \neq 0, \sigma} q b_{q\sigma}^\dagger b_{q\sigma} \quad (15)$$

the total momentum of the baths. This transformation acts as

$$U_{\text{LLP}}^\dagger d_{j\sigma} U_{\text{LLP}} = e^{-iajP_b} d_{j\sigma}, \quad (16a)$$

$$U_{\text{LLP}}^\dagger b_{q\sigma} U_{\text{LLP}} = e^{-iqX} b_{q\sigma}. \quad (16b)$$

Using the property that in a single-impurity subspace $d_{j\sigma}^\dagger d_{j\sigma} e^{iqX} = d_{j\sigma}^\dagger d_{j\sigma} e^{iqaj}$, we obtain

$$\begin{aligned} \mathcal{H}_{\text{LLP}} &= \sum_{p\sigma} E(p - P_b) d_{p\sigma}^\dagger d_{p\sigma} - J_\perp \sum_{p\sigma} d_{p\sigma}^\dagger d_{p\sigma} \\ &+ \sum_{q \neq 0, \sigma} v_\sigma |q| b_{q\sigma}^\dagger b_{q\sigma} \\ &+ \sum_{q \neq 0, \sigma} \frac{W_{q\sigma}}{L^{1/2}} \sum_j d_{j\sigma}^\dagger d_{j\sigma} (b_{q\sigma}^\dagger + b_{-q\sigma}). \end{aligned} \quad (17)$$

We can see that in this new basis the impurity momentum $P_d = \sum_{p\sigma} p d_{p\sigma}^\dagger d_{p\sigma}$ is now conserved. Indeed, the physical momentum operator in the LLP basis is $P_d^{\text{LLP}} \equiv U_{\text{LLP}}^\dagger P_d U_{\text{LLP}} = P_d - P_b$, which shows that $P_d = P_d^{\text{LLP}} + P_b = U_{\text{LLP}}^\dagger (P_d + P_b) U_{\text{LLP}} \equiv U_{\text{LLP}}^\dagger P_{\text{tot}} U_{\text{LLP}}$. In words, in the LLP basis the operator P_d coincides with the total polaron momentum, which is conserved. Notice that the physical impurity momentum is the one in the laboratory frame, i.e., before the LLP transformation, and it is obviously not conserved. As the dynamics does not couple different momentum sectors, we can work in a given sector, and substitute P_{tot} with its eigenvalue p . Then, the only ‘‘active’’ impurity degree of freedom is the bath index, that we describe via pseudospin variables

$$\sigma_i \equiv \sum_{p, \sigma, \sigma'} (\tau_i)_{\sigma\sigma'} d_{p\sigma}^\dagger d_{p\sigma'} = \sum_{j, \sigma, \sigma'} (\tau_i)_{\sigma\sigma'} d_{j\sigma}^\dagger d_{j\sigma'} \quad (18)$$

In the above equation, $(\tau_i)_{\sigma\sigma'}$ is the i th Pauli matrix. Taking into account that $\sum_{p\sigma} d_{p\sigma}^\dagger d_{p\sigma} = \mathbb{1}$ (i.e., there is only one impurity in the system), we can write

$$\begin{aligned} \mathcal{H}_{\text{LLP}}(p) &= \frac{(p - P_b)^2}{2M} - J_\perp \sigma_1 + \sum_{q \neq 0, \sigma} v_\sigma |q| b_{q\sigma}^\dagger b_{q\sigma} \\ &+ \sum_{q \neq 0, \sigma} \frac{W_{q\sigma}}{L^{1/2}} \frac{\mathbb{1} + \sigma \sigma_3}{2} (b_{q\sigma}^\dagger + b_{-q\sigma}). \end{aligned} \quad (19)$$

This final form of the Hamiltonian, that we will study in the following, is somewhat reminiscent of a spin-boson model [25].

III. OVERVIEW OF THE RESULTS

In the next section, we will study the dynamics of the model (19) using an improved, infinite-order perturbative expansion in the impurity-bath coupling $g_\sigma K_\sigma^{1/2}/v_\sigma$. Since the formalism is quite involved, we will start presenting the physical picture that emerges from the results we obtain. Throughout the paper, we will always assume that initially the baths are in their ground state $|\omega\rangle_b$, while the impurity is introduced in the system in an arbitrary wave packet

$$|\Psi(0)\rangle = \sum_{p,\mu \in \{e,o\}} c_{p\mu} |p, \mu\rangle_d |\omega\rangle_b, \quad (20)$$

where $|p, \mu\rangle_d = d_{p\mu}^\dagger |0\rangle_d$ are the free impurity eigenstates. When the baths are in the ground state the LLP transformation acts as the identity, so the state above can be considered as the representation of the wave function both in the laboratory and in the LLP frames.

The main achievement of this paper will be a perturbative expression of the state of the impurity and baths, which allows us to obtain the dynamics of the baths in response to the introduction and motion of the impurity. The advantage of having an approximate representation for the wave function is that we will be able to understand the dynamics of impurity and baths on the same footing. The case of a Gaussian impurity wave packet is illustrated in Fig. 2. In these plots, the contour lines depict the probability density of finding the impurity at a given position, while the color scale represents the fluctuation of the density of the baths. The plots on the left depict the $\sigma = 1$ (or \uparrow) bath, while the ones on the right represent the situation in the $\sigma = -1$ (\downarrow) bath. The impurity is initialized in a Gaussian wave packet with a standard deviation of position of about $12.5(Mv)^{-1}$ around the center of the \uparrow bath, with an average momentum $p_0 = 0.1Mv$.

The motion of the impurity is qualitatively similar to what we would expect in the absence of the interaction: the whole wave packet oscillates from one bath to the other, while drifting to the right because of the finite momentum. There is a little distortion in the shape of the wave packet, although the most prominent modification of its properties is not immediately noticeable from Fig. 2: unlike to the free impurity case, at every time $t > 0$ there is a nonvanishing probability to find the impurity in both baths. This property is visible in Fig. 2 as an elongation of the wave packets in the time direction, especially for later times (see also Sec. VIA for a discussion of this property). During the evolution, there is a net momentum transfer between impurity and baths, as detailed in Fig. 3. This momentum transfer is clearly seen also in the dynamics of the baths.

The latter evolve in an intuitive, semiclassical fashion: when the impurity appears for the first time in one of the baths, the latter responds by forming a density depletion in the position of the impurity, while at the same time two wave fronts form on its sides and propagate away at the speed of sound. Then, as the impurity oscillates from one bath to the other, the depth of the density depletion oscillates as well, and these oscillations propagate in the baths in the form of two trains of ripples. The wavelength of the latter corresponds to that of the phonons emitted from the decay of the odd mode of the impurity, which is different for backward and forward

emission because of the finite impurity momentum. Notice that the dynamics of the baths lags behind the time evolution of the impurity. This effect is particularly visible for larger interbath hopping [Figs. 2(a) and 2(b)], while for smaller J_\perp the baths and the impurity are almost synchronized [Figs. 2(c) and 2(d)].

The relation of the densities of the baths with the impurity density, presented in the figures above, can be understood by noticing that the equation of motion linking them at operator level is

$$\left(\frac{1}{v_\sigma^2} \partial_t^2 - \partial_x^2\right) \rho_\sigma(x, t) = \frac{g_\sigma K_\sigma}{\pi v_\sigma} \partial_x^2 N_\sigma(x, t), \quad (21)$$

where $N_\sigma(x) \equiv \sum_j \delta(x - ja) d_{j\sigma}^\dagger d_{j\sigma}$. The above equation is valid within the approximation that the bosonized density retains only the longest-wavelength contribution $-1/\pi \partial_x \phi_\sigma(x)$, which guarantees that the equations of motion for the densities are linear. Solving Eq. (21) one easily obtains

$$\begin{aligned} \rho_\sigma(x, t) &= \rho_\sigma(x, 0) \\ &+ g_\sigma \int_{\mathbb{R}} dx' \int_0^t dt' \chi_\sigma(x - x', t - t') N_\sigma(x', t'), \end{aligned} \quad (22)$$

where $\rho_\sigma(x, 0)$ is the noninteracting density at $t = 0$. The kernel $\chi_\sigma(x, t)$ is the retarded density-density linear response function for the baths,

$$\begin{aligned} \chi_\sigma(x, t) &\equiv -i\theta(t) \langle \omega | [\rho_\sigma(x, t), \rho_\sigma(0, 0)] | \omega \rangle \\ &= \theta(t) \frac{K_\sigma}{2\pi} [\delta'_\alpha(x + v_\sigma t) - \delta'_\alpha(x - v_\sigma t)], \end{aligned}$$

where the prime indicates a derivative with respect to the argument of the function

$$\delta_\alpha(x) \equiv \frac{1}{\pi} \frac{\alpha}{x^2 + \alpha^2}. \quad (23)$$

This function is a smeared representation of the Dirac delta function, whose smearing parameter α is the length that serves as a UV cutoff for the TLL.

If we take the average of Eq. (22) over the initial state $|\Psi(0)\rangle = |\chi\rangle_d |\omega\rangle_b$, we obtain the relation

$$\langle \rho_\sigma(x) \rangle_t = g_\sigma \int_{\mathbb{R}} dx' \int_0^t dt' \chi_\sigma(x - x', t - t') \langle N_\sigma(x') \rangle_{t'} \quad (24)$$

between the bath and impurity density. We have introduced the notation $\langle \mathcal{O}(x, t) \rangle \equiv \langle \mathcal{O}(x) \rangle_t$ to indicate the expectation value at time t of the operator $\mathcal{O}(x)$ in the Schrödinger picture. Substituting the expression for the retarded response function with $\alpha \rightarrow 0$ in the previous equation we get

$$\begin{aligned} \langle \rho_\sigma(x) \rangle_t &= \frac{g_\sigma K_\sigma}{2\pi} \int_0^t dt' [\partial_{x'} \langle N_\sigma(x') \rangle_{t'} |_{x'=x+v_\sigma(t-t')} \\ &- \partial_{x'} \langle N_\sigma(x') \rangle_{t'} |_{x'=x-v_\sigma(t-t')}], \end{aligned} \quad (25)$$

where the spatial arguments $x \pm v_\sigma(t - t')$ have to be interpreted modulo translation by the length of the system L because of the pbc. Although the above equation looks like a linear response formula, we stress that it is actually

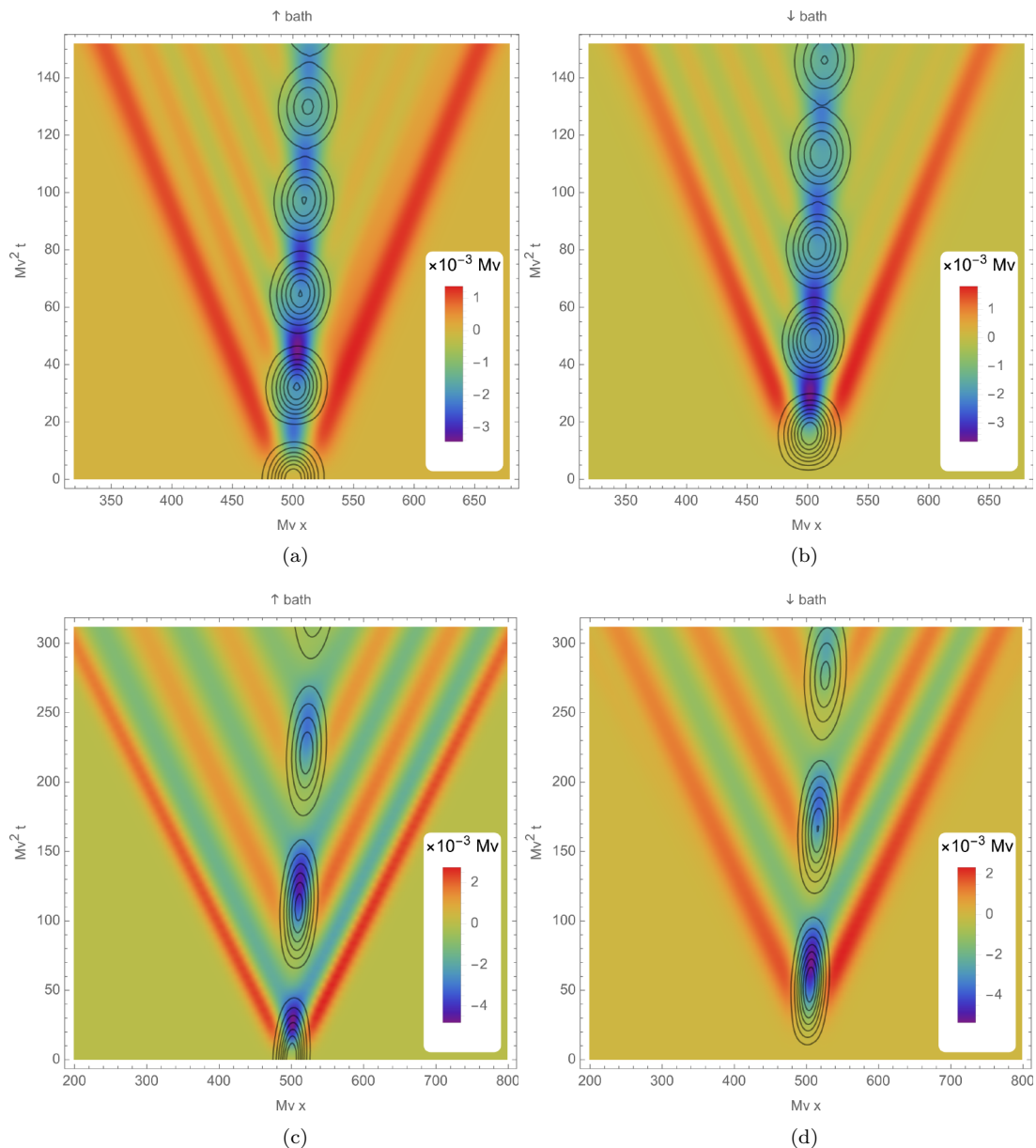


FIG. 2. Comparison of the dynamics of the density fluctuation in the baths (color scale) and of the impurity density (black contours) for $g^2K = 0.5v^2$ and [(a), (b)] $J_{\perp} = 0.1Mv^2$ or [(c), (d)] $J_{\perp} = 0.03Mv^2$. The dynamics of impurity and baths and are more synchronized for low J_{\perp} . The wave packet is Gaussian, composed of $N_p = 64$ momenta distributed around $p_0 = 0.1Mv$ with a standard deviation of $\delta p = 0.04Mv$. The system has a total length of $L = 1000(Mv)^{-1}$. The plots are not symmetric about $x = L/2$ because of the finite impurity momentum.

nonperturbative, because it comes from the Heisenberg equation of motion (21). It establishes an exact relation between the *interacting* impurity and bath density, valid within our long-wavelength description of the system. It shows that the bath density at coordinates (x, t) is a *superposition* of the all the values of the gradient of the impurity density on the light-cone of the given space-time point. Besides indicating that the baths have rather long “memory”, the superposition of the various images of the non-positive-definite gradient of the impurity density paves the way to interference effects. Equation (25) also provides a hint that the time evolution of the bath density will have a semiclassical character, in the sense that it follows the motion of the impurity.

In the following paragraphs, we will build a perturbative approximation of the time evolution of the system state. This solution will give us access to the dynamics of both the density of the impurity and of the baths, and we will observe the realization of the semiclassical behavior entailed by Eq. (25) [albeit Eq. (25) itself will be satisfied only approximately].

IV. THE PERTURBATIVE TECHNIQUE

We will now discuss the technique with which the results exposed in the previous section were obtained, and construct a perturbative expansion for the impurity-bath wave function. The first useful step is to rewrite the LPP in a given

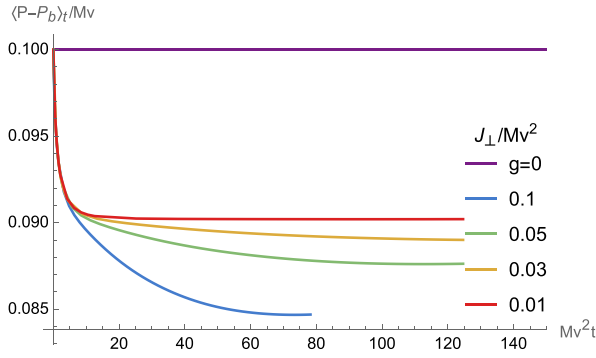


FIG. 3. Time evolution of the impurity momentum for the initial state $|p_0 \uparrow\rangle_d$, and symmetric baths. The plots are for $p_0 = 0.1Mv$, $g^2K = 0.5v^2$ and show the effect of increasing J_{\perp} . The $J_{\perp} = 0.1Mv^2$ curve is shown only within the time interval when the perturbative solution is valid.

momentum sector, Eq. (19) separating the *noninteracting* part $\mathcal{H}_0(p)$ and the perturbation V ,

$$\mathcal{H}_{\text{LLP}}(p) = \mathcal{H}_0(p) + \sigma_3 V + : \frac{P_b^2}{2M} :, \quad (26)$$

where the colons $: \cdot :$ stand for normal-ordering with respect to the phononic vacuum $|\omega\rangle$. The noninteracting Hamiltonian is

$$\mathcal{H}_0(p) = h_0(p) + E(p) - J_{\perp} \sigma_1, \quad (27)$$

with $h_0(p)$ being the bare bath Hamiltonian

$$h_0(p) \equiv \sum_{q \neq 0, \sigma} \left[\Omega_{q\sigma}(p) b_{q\sigma}^{\dagger} b_{q\sigma} + \frac{W_{q\sigma}}{2\sqrt{L}} (b_{q\sigma}^{\dagger} + b_{q\sigma}) \right], \quad (28)$$

and

$$\Omega_{q\sigma}(p) \equiv v_{\sigma} |q| - \frac{qP}{M} + \frac{q^2}{2M}. \quad (29)$$

The perturbation V is [26]

$$V = \sum_{q \neq 0, \sigma} \sigma \frac{W_{q\sigma}}{2\sqrt{L}} (b_{q\sigma}^{\dagger} + b_{q\sigma}). \quad (30)$$

The idea is to obtain a perturbative expansion for the time evolved wave function in powers of $g_{\sigma} K_{\sigma}^{1/2} / v_{\sigma}$, treating \mathcal{H}_0 as unperturbed Hamiltonian. We notice that \mathcal{H}_0 contains $g_{\sigma} K_{\sigma}^{1/2} / v_{\sigma}$, hence the resulting perturbative approximation will be actually of infinite order. A physical picture behind this choice is described in Appendix A. In intuitive terms, the unperturbed Hamiltonian contains the bath-induced transitions in which the band index (e, o) of the impurity does not change (intra-band transitions), whereas the $\sigma_3 V$ term describes inter-band transitions. We will apply the approach described in Ref. [27], that is designed to avoid the appearance of secular terms, i.e., terms that grow indefinitely in time, whose presence would invalidate the perturbative treatment [28].

Let us begin from the case in which the initial condition is factorized as $|p\mu\rangle_d |\omega\rangle_b \equiv |p\mu, \omega\rangle \equiv |\Psi_{p\mu}(0)\rangle$. Then, we go to a modified interaction picture

$$|\Psi_{p\mu}(t)\rangle = e^{-i\mathcal{H}_0 t} |\Psi_{p\mu}^I(t)\rangle = e^{-i\mathcal{H}_0 t} a_{p\mu}(t) |\phi_{p\mu}(t)\rangle, \quad (31)$$

in which the vector $|\Psi_{p\mu}^I(t)\rangle$ is split into a complex function $a_{p\mu}(t)$ and a state $|\phi_{p\mu}\rangle$. This splitting is specified imposing

$$\langle p\mu, \omega | \phi_{p\mu}(t) \rangle \equiv 1 \quad (32)$$

at all times, implying that

$$|\phi_{p\mu}(t)\rangle = |p\mu, \omega\rangle + |\delta\phi_{p\mu}(t)\rangle, \quad (33)$$

with $|\delta\phi_{p\mu}\rangle$ orthogonal to $|p\mu, \omega\rangle$. This condition ensures that secular terms will be resummed to all orders into $a_{p\mu}(t)$.

Substituting the equation above into the Schrödinger equation we obtain

$$i \frac{d}{dt} |\phi_{p\mu}(t)\rangle = (\Delta\mathcal{H}(t) - \Delta E_{p\mu}(t)) |\phi_{p\mu}(t)\rangle, \quad (34a)$$

$$i \frac{da_{p\mu}}{dt} = \Delta E_{p\mu}(t) a_{p\mu}, \quad a_{p\mu}(0) = 1, \quad (34b)$$

$$\Delta E_{p\mu}(t) \equiv \langle p\mu, \omega | \Delta\mathcal{H}(t) | \phi_{p\mu}(t) \rangle, \quad (34c)$$

where the equation for $a_{p\mu}$ is obtained by projecting onto $|p\mu, \omega\rangle$, and $\Delta\mathcal{H}(t)$ is the interaction-picture perturbation

$$\Delta\mathcal{H}(t) = e^{i\mathcal{H}_0 t} \left(\sigma_3 V + : \frac{P_b^2}{2M} : \right) e^{-i\mathcal{H}_0 t}. \quad (35)$$

Notice that we chose to treat $: P_b^2 / 2M$ as a perturbation, despite its formal independence from the coupling constant. This choice is justified when the initial bath state is the vacuum, as in this case the phonons modes will start to be populated only because of the interaction. This approach is akin to a spin-wave expansion in magnetic systems [29].

The equation for $a_{p\mu}$ is integrated straightforwardly,

$$a_{p\mu}(t) = e^{-i \int_0^t dt' \Delta E_{p\mu}(t')}. \quad (36)$$

The equation for $|\phi_{p\mu}(t)\rangle$ will in turn be solved perturbatively, assuming the expansion

$$|\delta\phi_{p\mu}\rangle = \sum_{n=1}^{\infty} |\phi_{p\mu}^{(n)}\rangle, \quad (37)$$

where $|\phi_{p\mu}^{(n)}\rangle = \mathcal{O}([g_{\sigma} K_{\sigma}^{1/2} / v_{\sigma}]^n)$. As usual in perturbative treatments, this Ansatz generates a hierarchy of equations for $|\phi_{p\mu}^{(n)}(t)\rangle$, which have to be solved by matching terms of the same order. Consequently, the function $\Delta E_{p\mu}(t)$ becomes a series in powers of the coupling, which is then substituted into Eq. (36). In our case, the matching of powers of $gK^{1/2}/v$ is nontrivial, because \mathcal{H}_0 already contains the coupling constant.

The details of the expansion can be now worked out order by order. The interaction-picture perturbation is

$$\Delta\mathcal{H}(t) = \sigma_3(t) \hat{V}(t) + \langle V(t) \rangle + : \frac{P_b^2}{2M} : (t). \quad (38)$$

Here [30]

$$\sigma_3(t) = \sum_{\mu=e/o} e^{-2i\mu J_{\perp} t} |p\mu\rangle \langle p\bar{\mu}|, \quad (39a)$$

$$\hat{V}(t) = \sum_{q \neq 0, \sigma} \sigma \frac{W_{q\sigma}}{2L^{1/2}} (b_{q\sigma} e^{-i\Omega_{q\sigma} t} + b_{q\sigma}^{\dagger} e^{i\Omega_{q\sigma} t}), \quad (39b)$$

$$\langle V(t) \rangle = -2 \sum_{q \neq 0, \sigma} \sigma \frac{W_{q\sigma}^2}{4L} \frac{1 - \cos \Omega_{q\sigma} t}{\Omega_{q\sigma}}. \quad (39c)$$

The last term originates from the inclusion of a term $\propto g_\sigma K_\sigma^{1/2}/v_\sigma$ in $h_0(p)$. Notice that

$$\sigma_3(t)|p\mu\rangle = e^{2i\mu J_\perp t}|p\bar{\mu}\rangle \quad (40)$$

where for $\mu = e/o$ we have $\bar{\mu} = o/e$.

Now we plug the expansion of $|\phi_{p\mu}\rangle$ in Eq. (34a). At first order, we have

$$i\frac{d}{dt}|\phi_{p\mu}^{(1)}(t)\rangle = (\Delta\mathcal{H}(t) - \Delta E_{p\mu}^{(1)}(t))|p\mu, \omega\rangle, \quad (41)$$

with

$$\Delta E_{p\mu}^{(1)}(t) = \langle p\mu, \omega|\Delta\mathcal{H}(t)|p\mu, \omega\rangle. \quad (42)$$

The action of $\Delta\mathcal{H}(t)$ on the initial state reads

$$\begin{aligned} \Delta\mathcal{H}(t)|p\mu, \omega\rangle &= \sum_{q\neq 0, \sigma} \sigma \frac{W_{q\sigma}}{2L^{1/2}} e^{i\Omega_{q\sigma}^+(p)t} b_{q\sigma}^\dagger |p\bar{\mu}, \omega\rangle \\ &+ e^{2i\mu J_\perp t} \langle V(t) \rangle |p\bar{\mu}, \omega\rangle + \frac{:P_b^2:}{2M}(t)|p\mu, \omega\rangle. \end{aligned} \quad (43)$$

We have introduced the convenient shorthands

$$\begin{aligned} \Omega_{q\sigma}^{\pm e}(p) &\equiv \Omega_{q\sigma}(p) \pm 2J_\perp, \\ \Omega_{q\sigma}^{\pm o}(p) &\equiv \Omega_{q\sigma}(p) \mp 2J_\perp. \end{aligned} \quad (44)$$

The lowest-order term generated by $\frac{:P_b^2:}{2M}(t)|p\mu, \omega\rangle$ is of order two, so it is easy to verify that $\Delta E_{p\mu}^{(1)}(t) = 0$. Moreover, we assume that $\frac{:P_b^2:}{2M}(t)|\phi_{p\mu}^{(1)}(t)\rangle$ is of second order, as well. We will

verify the consistency of this assumption *a posteriori*. Since $\langle V(t) \rangle$ is a second-order contribution we have that the first-order equation is simply

$$i\frac{d}{dt}|\phi_{p\mu}^{(1)}(t)\rangle = \sigma_3(t)\hat{V}(t)|p\mu, \omega\rangle, \quad (45)$$

which is straightforwardly integrated,

$$|\phi_{p\mu}^{(1)}(t)\rangle = \sum_{q\neq 0, \sigma} \sigma \frac{W_{q\sigma}}{2L^{1/2}} \frac{1 - e^{i\Omega_{q\sigma}^+ t}}{\Omega_{q\sigma}^+} b_{q\sigma}^\dagger |p\bar{\mu}\omega\rangle. \quad (46)$$

From the above equation, it can be verified that $\frac{:P_b^2:}{2M}(t)|\phi_{p\mu}^{(1)}(t)\rangle$ is of second order, as claimed before. The correct normalization of the state is guaranteed by computing $\Delta E_{p\mu}(t)$ to the second order,

$$\begin{aligned} \Delta E_{p\mu}(t) &= \Delta E_{p\mu}^{(2)}(t) = \langle \mu\omega|\sigma_3(t)\hat{V}(t)|\phi_{p\mu}^{(1)}(t)\rangle \\ &= - \sum_{q\neq 0, \sigma} \frac{W_{q\sigma}^2}{4L} \frac{1 - e^{-i\Omega_{q\sigma}^+ t}}{\Omega_{q\sigma}^+}. \end{aligned}$$

The normalization factor is

$$\begin{aligned} a_{p\mu}(t) &= e^{-i\int_0^t dt_1 \Delta E_{p\mu}^{(2)}(t_1)} \\ &= \exp\left(- \sum_{q\neq 0, \sigma} \frac{W_{q\sigma}^2}{4L} \frac{1 - i\Omega_{q\sigma}^+ t - e^{-i\Omega_{q\sigma}^+ t}}{(\Omega_{q\sigma}^+)^2}\right). \end{aligned} \quad (47)$$

The second-order correction is quite more involved. There is one contribution coming from the second term of Eq. (43),

$$\begin{aligned} |\delta_1\phi_{p\mu}^{(2)}(t)\rangle &= -i \int_0^t dt' e^{2i\mu J_\perp t'} \langle V(t') \rangle |p\bar{\mu}, \omega\rangle \\ &= \frac{1}{2\mu J_\perp} \sum_{q\neq 0, \sigma} \sigma \frac{W_{q\sigma}^2}{4L} [e^{2i\mu J_\perp t} 2\Re \chi_t(\Omega_{q\sigma}(p)) - \chi_t(\Omega_{q\sigma}^-(p)) - \chi_t^*(\Omega_{q\sigma}^+(p))] |p\bar{\mu}, \omega\rangle \\ &\equiv B_{p\mu}(t)|p\bar{\mu}, \omega\rangle. \end{aligned} \quad (48)$$

The other contribution involves bosonic creation operators and, in analogy with the first-order correction Eq. (46), it has the form

$$|\delta_2\phi_{p\mu}^{(2)}(t)\rangle = \sum_v \sum_{q\sigma, q'\sigma'} A_{q\sigma, q'\sigma'}^{\mu\nu}(p, t) b_{q\sigma}^\dagger b_{q'\sigma'}^\dagger |p\nu, \omega\rangle, \quad (49)$$

where $A_{q\sigma, q'\sigma'}^{\mu\nu}(p, t)$ is taken to be of order two, and symmetric upon exchange of $q\sigma$ with $q'\sigma'$. Then, it is easy to see that $:P_b^2/2M:(t)|\delta_2\phi_{p\mu}^{(2)}(t)\rangle$ generates a term of second order. Thus, the usual hierarchical structure of perturbative expansion (in which terms of order n are the sources for the next order) is lost, but the equation for $A_{q\sigma, q'\sigma'}^{\mu\nu}(t)$ is still solvable. The details can be found in Appendix C, here we only quote the results,

$$\begin{aligned} A_{q\sigma, q'\sigma'}^{\mu\nu}(p, t) &= \frac{W_{q\sigma} W_{q'\sigma'}}{4L} \left\{ \frac{qq'}{2M} \frac{1}{\Omega_{q\sigma} \Omega_{q'\sigma'}} \left[e^{i\Omega_{q\sigma} t} \chi_t \left(\Omega_{q\sigma} + \frac{qq'}{M} \right) + e^{i\Omega_{q'\sigma'} t} \chi_t \left(\Omega_{q'\sigma'} + \frac{qq'}{M} \right) \right. \right. \\ &- \chi_t \left(\frac{qq'}{M} \right) - e^{i(\Omega_{q\sigma} + \Omega_{q'\sigma'}) t} \chi_t \left(\Omega_{q\sigma} + \Omega_{q'\sigma'} + \frac{qq'}{M} \right) \left. \right] \\ &+ \frac{\sigma\sigma'}{2} \left[\frac{1}{\Omega_{q'\sigma'}^+} \left(e^{i(\Omega_{q\sigma} + \Omega_{q'\sigma'}) t} \chi_t \left(\Omega_{q\sigma} + \Omega_{q'\sigma'} + \frac{qq'}{M} \right) - e^{i\Omega_{q\sigma}^- t} \chi_t \left(\Omega_{q\sigma}^- + \frac{qq'}{M} \right) \right) \right. \\ &\left. \left. + \frac{1}{\Omega_{q\sigma}^+} \left(e^{i(\Omega_{q\sigma} + \Omega_{q'\sigma'}) t} \chi_t \left(\Omega_{q\sigma} + \Omega_{q'\sigma'} + \frac{qq'}{M} \right) - e^{i\Omega_{q'\sigma'}^- t} \chi_t \left(\Omega_{q'\sigma'}^- + \frac{qq'}{M} \right) \right) \right] \right\} \quad (50) \end{aligned}$$

$$\begin{aligned}
A_{q\sigma, q'\sigma'}^{\mu\bar{\mu}}(p, t) = & \frac{1}{2} \frac{W_{q\sigma} W_{q'\sigma'}}{4L} \left\{ \frac{\sigma}{\Omega_{q\sigma}^{+\mu} \Omega_{q'\sigma'}} \left[e^{i\Omega_{q\sigma}^{+\mu} t} \chi_t \left(\Omega_{q\sigma}^{+\mu} + \frac{qq'}{M} \right) + e^{i\Omega_{q'\sigma'} t} \chi_t \left(\Omega_{q'\sigma'} + \frac{qq'}{M} \right) \right. \right. \\
& - \left. \chi_t \left(\frac{qq'}{M} \right) - e^{i(\Omega_{q\sigma}^{+\mu} + \Omega_{q'\sigma'}) t} \chi_t \left(\Omega_{q\sigma}^{+\mu} + \Omega_{q'\sigma'} + \frac{qq'}{M} \right) \right] + \frac{\sigma'}{\Omega_{q'\sigma'}^{+\mu} \Omega_{q\sigma}} \\
& \times \left[e^{i\Omega_{q'\sigma'}^{+\mu} t} \chi_t \left(\Omega_{q'\sigma'}^{+\mu} + \frac{qq'}{M} \right) + e^{i\Omega_{q\sigma} t} \chi_t \left(\Omega_{q\sigma} + \frac{qq'}{M} \right) - \chi_t \left(\frac{qq'}{M} \right) - e^{i(\Omega_{q\sigma} + \Omega_{q'\sigma'}^{+\mu}) t} \chi_t \left(\Omega_{q\sigma} + \Omega_{q'\sigma'}^{+\mu} + \frac{qq'}{M} \right) \right] \left. \right\}. \quad (51)
\end{aligned}$$

In the above equations, all $\Omega_{q\sigma}$ s and $\Omega_{q\sigma}^{\pm\mu}$ are evaluated at momentum p , and we defined the function

$$\chi_t(\varepsilon) \equiv \frac{1 - e^{-i\varepsilon t}}{\varepsilon}. \quad (52)$$

To sum up, when $|\Psi_{p\mu}(0)\rangle = |p\mu, \omega\rangle$, the state evolution is approximated by

$$\begin{aligned}
|\Psi_{p\mu}(t)\rangle = & a_{p\mu}(t) e^{-ih_0(p)t} \left[e^{-i\lambda_{p\mu} t} |p\mu, \omega\rangle + e^{-i\lambda_{p\bar{\mu}} t} \sum_{q \neq 0, \sigma} \sigma \frac{W_{q\sigma}}{2L^{1/2}} \frac{1 - e^{-i\Omega_{q\sigma}^{+\mu}(p)t}}{\Omega_{q\sigma}^{+\mu}(p)} b_{q\sigma}^\dagger |p\bar{\mu}, \omega\rangle \right. \\
& \left. + e^{-i\lambda_{p\bar{\mu}} t} B_{p\mu}(t) |p\bar{\mu}, \omega\rangle + \sum_v \sum_{q\sigma, q'\sigma'} e^{-i\lambda_{pv} t} A_{q\sigma, q'\sigma'}^{\mu\nu}(p, t) b_{q\sigma}^\dagger b_{q'\sigma'}^\dagger |pv, \omega\rangle \right]. \quad (53)
\end{aligned}$$

Letting $e^{-ih_0(p)t}$ act on the bath states, we can also write

$$\begin{aligned}
|\Psi_{p\mu}(t)\rangle = & a_{p\mu}(t) \left[e^{-i\lambda_{p\mu} t} |p\mu\rangle |\omega_p(t)\rangle - e^{-i(\lambda_{p\bar{\mu}} - 2\mu J_\perp)t} \sum_{q \neq 0, \sigma} \sigma \frac{W_{q\sigma}}{2L^{1/2}} \frac{1 - e^{-i\Omega_{q\sigma}^{+\mu}(p)t}}{\Omega_{q\sigma}^{+\mu}(p)} b_{q\sigma}^\dagger |p\bar{\mu}\rangle |\omega_p(t)\rangle \right. \\
& \left. + e^{-i\lambda_{p\bar{\mu}} t} \tilde{B}_{p\mu}(t) |p\bar{\mu}\rangle |\omega_p(t)\rangle + \sum_v \sum_{q\sigma, q'\sigma'} e^{-i\lambda_{pv} t} A_{q\sigma, q'\sigma'}^{\mu\nu}(p) e^{-i(\Omega_{q\sigma}(p) + \Omega_{q'\sigma'}(p))t} b_{q\sigma}^\dagger b_{q'\sigma'}^\dagger |pv\rangle |\omega_p(t)\rangle \right], \quad (54)
\end{aligned}$$

where

$$\begin{aligned}
|\omega_p(t)\rangle & \equiv e^{-ih_0 t} |\omega\rangle \\
& = e^{i\alpha_p(t)} \left| \text{coh} \left[-\frac{W_{q\sigma}}{2L^{1/2}} \frac{1 - e^{-i\Omega_{q\sigma}(p)t}}{\Omega_{q\sigma}(p)} \right] \right\rangle, \quad (55)
\end{aligned}$$

is the ‘‘zeroth order’’ evolution of the initial bath state. The notation $|\text{coh}[z_{q\sigma}]\rangle$ means a coherent state

$$|\text{coh}[z_{q\sigma}]\rangle \equiv e^{\sum_{q \neq 0, \sigma} (z_{q\sigma} b_{q\sigma}^\dagger - z_{q\sigma}^* b_{q\sigma})} |\omega\rangle, \quad (56)$$

and the phase is

$$\alpha_p(t) \equiv \sum_{q \neq 0, \sigma} \frac{W_{q\sigma}^2}{4L} \frac{\Omega_{q\sigma}(p)t - \sin(\Omega_{q\sigma}(p)t)}{(\Omega_{q\sigma}(p))^2}. \quad (57)$$

Notice that commuting $e^{-ih_0(p)t}$ with $b_{p\sigma}^\dagger$ introduces a shift in $B_{p\mu}(t)$, hence in Eq. (54) we have

$$\tilde{B}_{p\mu}(t) = B_{p\mu}(t) - \sum_{q \neq 0, \sigma} \sigma \frac{W_{q\sigma}^2}{4L} \chi_t^*(\Omega_{q\sigma}^{+\mu}(p)) \chi_t(\Omega_{q\sigma}(p)). \quad (58)$$

The analogous shifts in the last term of Eq. (54) have been neglected for consistency, since they result in higher-order contributions in our small parameter. The shift above is logarithmically divergent in the TLL cutoff, and vanishes whenever the two baths are identical, that is, they have the same properties (v_σ , K_σ , g_σ). In the following, we will

work mainly in this symmetric case, hence we will soon discard it.

The perturbative solution (54) has a clear physical interpretation: The state evolution is approximated by the emission of phonons from the deexcitation $|\omega\rangle \rightarrow |e\rangle$ above a coherent-state background, which will turn out to embody the orthogonality catastrophe. The solution is also reminiscent of a popular Ansatz used to describe Fermi polarons in higher dimensions, in which the impurity state is expanded in terms with an increasing number of particle-hole pairs excited from the Fermi sphere [11,31]. As the TLL bosons are descendants of particle-hole pairs, we see that the expression in Eq. (54) is indeed the 1D analog of the above-mentioned Ansatz, albeit it is perturbative and not variational in nature. The main difference between the two is that instead of adding excitations on the Fermi sphere (i.e., the bosonic ground state $|\omega\rangle$), in Eq. (54) the bosons are added on top of a coherent state, which embodies the physics of the OC.

From the above results, the time evolution of a wave packet $|\Psi(0)\rangle = \sum_{p\mu} c_{p\mu} |p\mu, \omega\rangle$ is simply given by the superposition of Eq. (53) or (54),

$$|\Psi(t)\rangle = \sum_{p\mu} e^{-i\lambda_{p\mu}t} |p\mu\rangle e^{-ih_0(p)t} \left[(c_{p\mu} a_{p\mu} + c_{p\bar{\mu}} a_{p\bar{\mu}} B_{p\bar{\mu}}(t)) |\omega\rangle + c_{p\bar{\mu}} a_{p\bar{\mu}} \sum_{q \neq 0, \sigma} \sigma \frac{W_{q\sigma}}{2L^{1/2}} \frac{1 - e^{i\Omega_{q\sigma}^- t}}{\Omega_{q\sigma}^-} b_{q\sigma}^\dagger |\omega\rangle \right. \\ \left. + \sum_{q\sigma, q'\sigma'} (c_{p\mu} a_{p\mu} A_{q\sigma, q'\sigma'}^{\mu\mu}(p, t) + c_{p\bar{\mu}} a_{p\bar{\mu}} A_{q\sigma, q'\sigma'}^{\bar{\mu}\mu}(p, t)) b_{q\sigma}^\dagger b_{q'\sigma'}^\dagger |\omega\rangle \right], \quad (59)$$

or

$$|\Psi(t)\rangle = \sum_{p\mu} e^{-i\lambda_{p\mu}t} |p\mu\rangle \left[(c_{p\mu} a_{p\mu} + c_{p\bar{\mu}} a_{p\bar{\mu}} \tilde{B}_{p\bar{\mu}}(t)) |\omega_p(t)\rangle + c_{p\bar{\mu}} a_{p\bar{\mu}} e^{-2i\mu J_\perp t} \sum_{q \neq 0, \sigma} \sigma \frac{W_{q\sigma}}{2L^{1/2}} \frac{1 - e^{-i\Omega_{q\sigma}^- t}}{\Omega_{q\sigma}^-} b_{q\sigma}^\dagger |\omega_p(t)\rangle \right. \\ \left. + \sum_{q\sigma, q'\sigma'} (c_{p\mu} a_{p\mu} A_{q\sigma, q'\sigma'}^{\mu\mu}(p, t) + c_{p\bar{\mu}} a_{p\bar{\mu}} A_{q\sigma, q'\sigma'}^{\bar{\mu}\mu}(p, t)) e^{-i(\Omega_{q\sigma}(p) + \Omega_{q'\sigma'}(p))t} b_{q\sigma}^\dagger b_{q'\sigma'}^\dagger |\omega_p(t)\rangle \right]. \quad (60)$$

The calculation and characterization of the normalization factors $a_{p\mu}(t)$ can be found in Appendix B. For now, we just point out that they have the long-time asymptotic behaviors

$$a_{pe}(t) \sim e^{z_{pe} - i\Delta\lambda_{pe}t + \mathcal{O}(1/t)} \quad (61a)$$

$$a_{po}(t) \sim e^{z_{po} - i\Delta\lambda_{po}t - 2\gamma_p t + \mathcal{O}(1/t)}, \quad (61b)$$

where $z_{p\mu}$ are two complex constants, $\Delta\lambda_{p\mu}$ are the interaction-induced shifts of the band energies, and $2\gamma_p$ is the decay constant of the odd mode. The expressions of these functions can be found in the above-mentioned Appendix B. The behaviors in Eqs. (61) are established rather quickly (for small momentum $|p| \lesssim 0.5Mv$, already for $J_\perp t \sim 0.1$). The expressions for the parameters appearing in the equations above can be found in Appendix B.

We remark that the validity of the perturbative solution is limited in time because the state normalization is guaranteed only up to the fourth order. As a consequence, the maximum time before the normalization is significantly lost is of the order of the odd mode decay time, $1/(2\gamma_p)$, which is usually much longer than the period of the hopping between baths.

As a check of the reliability of this solution, we calculated the ‘‘Green’s function’’ $G_{\parallel}(p, t) = -i\langle p\sigma, \omega | e^{-i\mathcal{H}t} | p\sigma, \omega \rangle$ and compared the result with the one from the linked cluster expansion (previously computed by the present authors in [15]), finding perfect agreement in the symmetric case. More details can be found in Appendix D

V. OBSERVABLES

In this section, we report the expressions of some interesting observables of the impurity-baths systems, obtained from our perturbative solution Eqs. (59) or (60).

A. Impurity observables

The simplest observable is the probability that the impurity is found in the bath σ , which is the expectation value of the operator

$$n_\sigma \equiv \sum_j d_{j\sigma}^\dagger d_{j\sigma}. \quad (62)$$

After the LLP transformation, it reads [compare with Eq. (17) and Eq. (19)]

$$n_\sigma = \frac{1}{2}(1 + \sigma\sigma_3). \quad (63)$$

Using the notation

$$|\Psi(t)\rangle = \sum_{p\mu} |p\mu\rangle_d |\psi_{p\mu}(t)\rangle_b \quad (64)$$

for the evolved state (notice that the bath states are not normalized to one), we find [32]

$$\langle n_\sigma \rangle_t = \frac{1}{2} + \frac{\sigma}{2} \sum_{p\mu} \langle \psi_{p\mu}(t) | \psi_{p\bar{\mu}}(t) \rangle, \quad (65)$$

where $\langle \cdot \rangle_t \equiv \langle \Psi(t) | \cdot | \Psi(t) \rangle$. The overlaps are easily calculated to be

$$\langle \psi_{p\mu}(t) | \psi_{p\bar{\mu}}(t) \rangle = e^{-2i\mu J_\perp t} [(c_{p\mu} a_{p\mu})^* c_{p\bar{\mu}} a_{p\bar{\mu}} + |c_{p\bar{\mu}} a_{p\bar{\mu}}|^2 \tilde{B}_{p\bar{\mu}}^*(t) + |c_{p\mu} a_{p\mu}|^2 \tilde{B}_{p\mu}(t)] \\ + |c_{p\mu} a_{p\mu}|^2 \sum_{q \neq 0, \sigma} \sigma \frac{W_{q\sigma}^2}{4L} \frac{1 - e^{i\Omega_{q\sigma}(p)t}}{\Omega_{q\sigma}(p)} \frac{1 - e^{-i\Omega_{q\sigma}^+(p)t}}{\Omega_{q\sigma}^+(p)} + |c_{p\bar{\mu}} a_{p\bar{\mu}}|^2 \sum_{q \neq 0, \sigma} \sigma \frac{W_{q\sigma}^2}{4L} \frac{1 - e^{i\Omega_{q\sigma}^-(p)t}}{\Omega_{q\sigma}^-(p)} \frac{1 - e^{-i\Omega_{q\sigma}(p)t}}{\Omega_{q\sigma}(p)} \\ + e^{2i\mu J_\perp t} (c_{p\bar{\mu}} a_{p\bar{\mu}})^* c_{p\mu} a_{p\mu} \sum_{q \neq 0, \sigma} \frac{W_{q\sigma}^2}{4L} \frac{1 - e^{i\Omega_{q\sigma}^-(p)t}}{\Omega_{q\sigma}^-(p)} \frac{1 - e^{-i\Omega_{q\sigma}^+(p)t}}{\Omega_{q\sigma}^+(p)} + \mathcal{O}((gK^{1/2}/v)^3) \quad (66)$$

at second order.

In problems concerning mobile impurities, a natural observable to be considered is the impurity momentum. In the LLP basis, it reads $P_d = P - P_b$, so, since P is a constant of motion, all that is required to compute is the momentum carried by the baths. The latter is given by

$$\begin{aligned} \langle P_b \rangle_t &= \sum_{q \neq 0, \sigma} q \langle b_{q\sigma}^\dagger b_{q\sigma} \rangle_t \\ &= 2 \sum_{p\mu} |c_{p\mu} a_{p\mu}|^2 \sum_{q \neq 0, \sigma} q \frac{W_{q\sigma}^2}{4L} \frac{1 - \cos \Omega_{q\sigma}^{+\mu}(p)t}{(\Omega_{q\sigma}^{+\mu}(p))^2} + 2\Re \left[\sum_{p\mu} (c_{p\mu} a_{p\mu})^* c_{p\bar{\mu}} a_{p\bar{\mu}} \right. \\ &\quad \left. \times \sum_{q \neq 0, \sigma} \sigma q \frac{W_{q\sigma}^2}{4L} \frac{1 - e^{-i\Omega_{q\sigma}(p)t}}{\Omega_{q\sigma}(p)} \frac{1 - e^{i\Omega_{q\sigma}^{-\mu}(p)t}}{\Omega_{q\sigma}^{-\mu}(p)} \right] + 2 \sum_{p\mu} |c_{p\mu}|^2 \sum_{q \neq 0, \sigma} q \frac{W_{q\sigma}^2}{4L} \frac{1 - \cos \Omega_{q\sigma}(p)t}{(\Omega_{q\sigma}(p))^2} \end{aligned} \quad (67)$$

The sums over the bath momenta can be converted into energy integrals by introducing the appropriate density of states

$$\begin{aligned} \frac{1}{L} \sum_{q \neq 0} q W_{q\sigma}^2 f(\Omega_{q\sigma}(p)) &= \int d\varepsilon R_1^\sigma(\varepsilon; p) f(\varepsilon), \\ R_1^\sigma(\varepsilon; p) &\equiv \frac{1}{L} \sum_{q \neq 0} q W_{q\sigma}^2 \delta(\varepsilon - \Omega_{q\sigma}(p)), \end{aligned}$$

which in the continuum limit is given by

$$R_1^\sigma(\varepsilon; p) = \frac{M^2 \tilde{g}_\sigma^2}{(2\pi)^2} \theta(\varepsilon) e^{-\varepsilon/\Lambda} \sum_{s=\pm 1} \left[-s \left(v_\sigma + s \frac{p}{M} \right) \right] \left[\left(1 + \frac{\varepsilon}{k_{s\sigma}(p)} \right)^{1/2} - 2 + \left(1 + \frac{\varepsilon}{k_{s\sigma}(p)} \right)^{-1/2} \right]. \quad (68)$$

The expression in Eq. (67) is composed of three contributions. The first two are contributions coming from the deexcitation of the odd mode, as signaled by their explicit dependence on J_\perp . The second of these two accounts for the asymmetries in the bath index, as it vanishes if the baths are symmetric or if the impurity is initialized in one of its noninteracting eigenstates. The last part of Eq. (67) comes from the coherent background $|\omega_p(t)\rangle$ term of the baths state, and is independent of the initial bath index of the impurity. It quantifies the momentum adsorbed by the baths as they adjust to the injection of the impurity.

Finally, we can calculate the probability of finding the impurity at the site j and in the bath σ , namely the expectation

value of the number operator $d_{j\sigma}^\dagger d_{j\sigma}$. The latter is invariant under the LLP transformation [see Eq. (16)]. Using $d_{j\sigma}^\dagger d_{j\sigma} = N^{-1} \sum_p e^{ipaj} \sum_k d_{k-p\sigma}^\dagger d_{k\sigma}$ and $d_{p\sigma} = (d_{pe} + \sigma d_{p\sigma})/\sqrt{2}$ we find

$$\langle d_{j\sigma}^\dagger d_{j\sigma} \rangle_t = \frac{1}{2N} \sum_p e^{ipja} \sum_{k,\mu} (\langle \psi_{k-p\mu} | \psi_{k\mu} \rangle + \sigma \langle \psi_{k-p\mu} | \psi_{k\bar{\mu}} \rangle). \quad (69)$$

Notice that Eq. (69) correctly reproduces Eq. (65) when summed on all sites. The fundamental ingredients of the above equation are the overlaps of the bath states, which read

$$\begin{aligned} \langle \psi_{p\mu} | \psi_{k\mu} \rangle &= e^{i(E_p - E_k)t} \langle \omega_p(t) | \omega_k(t) \rangle \left[(c_{p\mu} a_{p\mu})^* c_{k\mu} a_{k\mu} + (c_{p\bar{\mu}} a_{p\bar{\mu}})^* c_{k\mu} a_{k\mu} \tilde{B}_{p\bar{\mu}}^* + (c_{p\mu} a_{p\mu})^* c_{k\bar{\mu}} a_{k\bar{\mu}} \tilde{B}_{k\bar{\mu}} + e^{-i\mu 2J_\perp t} (c_{p\mu} a_{p\mu})^* \right. \\ &\quad \times c_{k\bar{\mu}} a_{k\bar{\mu}} \sum_{q \neq 0, \sigma} \sigma \frac{W_{q\sigma}^2}{4L} \frac{1 - e^{i\Omega_{q\sigma}(p)t}}{\Omega_{q\sigma}(p)} \frac{1 - e^{-i\Omega_{q\sigma}^{-\mu}(k)t}}{\Omega_{q\sigma}^{-\mu}(k)} + e^{i\mu 2J_\perp t} (c_{p\bar{\mu}} a_{p\bar{\mu}})^* c_{k\mu} a_{k\mu} \sum_{q \neq 0, \sigma} \sigma \frac{W_{q\sigma}^2}{4L} \frac{1 - e^{i\Omega_{q\sigma}^{-\mu}(p)t}}{\Omega_{q\sigma}^{-\mu}(p)} \frac{1 - e^{-i\Omega_{q\sigma}(k)t}}{\Omega_{q\sigma}(k)} \\ &\quad \left. + (c_{p\bar{\mu}} a_{p\bar{\mu}})^* c_{k\bar{\mu}} a_{k\bar{\mu}} \sum_{q \neq 0, \sigma} \frac{W_{q\sigma}^2}{4L} \frac{1 - e^{i\Omega_{q\sigma}^{-\mu}(p)t}}{\Omega_{q\sigma}^{-\mu}(p)} \frac{1 - e^{-i\Omega_{q\sigma}^{-\mu}(k)t}}{\Omega_{q\sigma}^{-\mu}(k)} + \mathcal{O}((gK^{1/2}/v)^3) \right], \end{aligned} \quad (70a)$$

$$\begin{aligned} \langle \psi_{p\mu} | \psi_{k\bar{\mu}} \rangle &= e^{i(E_p - E_k - \mu 2J_\perp)t} \langle \omega_p(t) | \omega_k(t) \rangle \left[(c_{p\mu} a_{p\mu})^* c_{k\bar{\mu}} a_{k\bar{\mu}} + (c_{p\bar{\mu}} a_{p\bar{\mu}})^* c_{k\bar{\mu}} a_{k\bar{\mu}} \tilde{B}_{p\bar{\mu}}^* + (c_{p\mu} a_{p\mu})^* c_{k\mu} a_{k\mu} \tilde{B}_{k\mu} \right. \\ &\quad \left. + e^{i\mu 2J_\perp t} (c_{p\mu} a_{p\mu})^* c_{k\mu} a_{k\mu} \sum_{q \neq 0, \sigma} \sigma \frac{W_{q\sigma}^2}{4L} \frac{1 - e^{i\Omega_{q\sigma}(p)t}}{\Omega_{q\sigma}(p)} \frac{1 - e^{-i\Omega_{q\sigma}^{+\mu}(k)t}}{\Omega_{q\sigma}^{+\mu}(k)} + e^{i\mu 2J_\perp t} (c_{p\bar{\mu}} a_{p\bar{\mu}})^* c_{k\bar{\mu}} a_{k\bar{\mu}} \right] \end{aligned}$$

$$\begin{aligned} & \times \sum_{q \neq 0, \sigma} \sigma \frac{W_{q\sigma}^2}{4L} \frac{1 - e^{i\Omega_{q\sigma}^-(p)t}}{\Omega_{q\sigma}^-(p)} \frac{1 - e^{-i\Omega_{q\sigma}(k)t}}{\Omega_{q\sigma}(k)} + e^{i4\mu J_{\perp} t} (c_{p\bar{\mu}} a_{p\bar{\mu}})^* c_{k\mu} a_{k\mu} \\ & \times \sum_{q \neq 0, \sigma} \frac{W_{q\sigma}^2}{4L} \frac{1 - e^{i\Omega_{q\sigma}^-(p)t}}{\Omega_{q\sigma}^-(p)} \frac{1 - e^{-i\Omega_{q\sigma}^+(k)t}}{\Omega_{q\sigma}^+(k)} + \mathcal{O}((gK^{1/2}/v)^3) \Big], \end{aligned} \quad (70b)$$

where the coherent-states overlap is given by

$$\ln \langle \omega_p(t) | \omega_k(t) \rangle = -\frac{1}{4L} \sum_{q \neq 0, \sigma} W_{q\sigma}^2 \left[\frac{1 + i\Omega_{q\sigma}(p)t - e^{i\Omega_{q\sigma}(p)t}}{(\Omega_{q\sigma}(p))^2} + \frac{1 - i\Omega_{q\sigma}(k)t - e^{-i\Omega_{q\sigma}(k)t}}{(\Omega_{q\sigma}(k))^2} - \frac{1 - e^{i\Omega_{q\sigma}(p)t}}{\Omega_{q\sigma}(p)} \frac{1 - e^{-i\Omega_{q\sigma}(k)t}}{\Omega_{q\sigma}(k)} \right]. \quad (71)$$

For any $p \neq k$ it has a slow, power-law decrease in time and it is a nonanalytic function of the momenta in $p = k$. Of course, for $p = k$ it is identically equal to 1 [as $|\omega_p(t)\rangle$ is normalized], which is also its maximum absolute value.

B. Bath observables

We will look at correlation functions of the bath densities $\rho_{\sigma}(x)$ and conjugate momenta [20] $\Pi_{\sigma}(x) \equiv 1/\pi d\theta_{\sigma}(x)/dx$,

$$\begin{aligned} \rho_{\sigma}(x) &= -\frac{1}{\pi} \frac{d}{dx} \phi_{\sigma}(x) \\ &= \frac{K_{\sigma}^{1/2}}{L^{1/2}} \sum_{q \neq 0} V_q (e^{iqx} b_{q\sigma} + e^{-iqx} b_{q\sigma}^{\dagger}), \end{aligned} \quad (72a)$$

$$\begin{aligned} \Pi_{\sigma}(x) &= \frac{1}{\pi} \frac{d}{dx} \theta_{\sigma}(x) \\ &= \frac{1}{K_{\sigma}^{1/2} L^{1/2}} \sum_{q \neq 0} \text{sgn}(q) V_q (e^{iqx} b_{q\sigma} + e^{-iqx} b_{q\sigma}^{\dagger}), \end{aligned} \quad (72b)$$

where $\text{sgn}(q)$ is the sign function. We remark that we understand $\rho_{\sigma}(x)$ as the fluctuation part of the density, that is, we already subtracted the average density $\bar{\rho}_{\sigma}$ from it [33]. In order to use the perturbative solution we found, we must first perform a LLP transformation [Eq. (16)], which replaces $b_{q\sigma} \rightarrow b_{q\sigma} e^{-iqX}$. Therefore, we have

$$\langle \rho_{\sigma}(x) \rangle_t = 2\Re \left[\frac{K_{\sigma}^{1/2}}{L^{1/2}} \sum_{q \neq 0} V_q e^{iqx} \langle e^{-iqX} b_{q\sigma} \rangle_t \right], \quad (73a)$$

$$\langle \Pi_{\sigma}(x) \rangle_t = 2\Re \left[\frac{1}{K_{\sigma}^{1/2} L^{1/2}} \sum_{q \neq 0} \text{sgn}(q) V_q e^{iqx} \langle e^{-iqX} b_{q\sigma} \rangle_t \right]. \quad (73b)$$

Using expression (59) [or (60)] and the property that $e^{-iqX} |p\mu\rangle = |p - q\mu\rangle$, we find

$$\begin{aligned} \langle e^{-iqX} b_{q\sigma} \rangle_t &= -\frac{W_{q\sigma}}{2L^{1/2}} \sum_{p\mu} e^{i(E_{p-q} - E_p)t} \langle \omega_{p-q}(t) | \omega_p(t) \rangle (c_{p-q, \mu} a_{p-q, \mu}(t))^* [c_{p\mu} a_{p\mu}(t) \chi_t(\Omega_{q\sigma}(p)) \\ &+ \sigma e^{-i\mu 2J_{\perp} t} c_{p\bar{\mu}} a_{p\bar{\mu}}(t) \chi_t(\Omega_{q\sigma}^-(p))] + \mathcal{O}((gK^{1/2}/v)^3), \end{aligned} \quad (74)$$

at the lowest order. It can be seen immediately that the two densities $\langle \rho_{\sigma}(x) \rangle_t$ and $\langle \Pi_{\sigma}(x) \rangle_t$ vanish unless the initial impurity state contains more than one momentum. This situation is physically consistent with the intuition that the impurity in a well-defined momentum state is equally distributed along the bath(s).

As the impurity is exchanged between the baths, these will become correlated. We will measure the amount of interbath correlation by computing the equal-time connected correlation functions

$$\begin{aligned} \langle \rho_{\sigma}(x) \rho_{\bar{\sigma}}(y) \rangle_t^c &\equiv \langle \rho_{\sigma}(x) \rho_{\bar{\sigma}}(y) \rangle_t - \langle \rho_{\sigma}(x) \rangle_t \langle \rho_{\bar{\sigma}}(y) \rangle_t, \\ \langle \Pi_{\sigma}(x) \Pi_{\bar{\sigma}}(y) \rangle_t^c &\equiv \langle \Pi_{\sigma}(x) \Pi_{\bar{\sigma}}(y) \rangle_t - \langle \Pi_{\sigma}(x) \rangle_t \langle \Pi_{\bar{\sigma}}(y) \rangle_t, \end{aligned} \quad (75)$$

whose expressions are

$$\langle \rho_\sigma(x) \rho_{\bar{\sigma}}(y) \rangle_t = (K_\sigma K_{\bar{\sigma}})^{1/2} 2\Re \left\{ \frac{1}{L} \sum_{q, \bar{q} \neq 0} V_q V_{\bar{q}} [\langle b_{q\sigma} b_{\bar{q}\bar{\sigma}} e^{-i(q+\bar{q})X} \rangle_t e^{i(qx+\bar{q}y)} + \langle b_{q\sigma}^\dagger b_{\bar{q}\bar{\sigma}} e^{i(q-\bar{q})X} \rangle_t e^{-i(qx-\bar{q}y)}] \right\}, \quad (76a)$$

$$\langle \Pi_\sigma(x) \Pi_{\bar{\sigma}}(y) \rangle_t = (K_\sigma K_{\bar{\sigma}})^{-1/2} 2\Re \left\{ \frac{1}{L} \sum_{q, \bar{q} \neq 0} V_q V_{\bar{q}} \text{sgn}(q\bar{q}) [\langle b_{q\sigma} b_{\bar{q}\bar{\sigma}} e^{-i(q+\bar{q})X} \rangle_t e^{i(qx+\bar{q}y)} + \langle b_{q\sigma}^\dagger b_{\bar{q}\bar{\sigma}} e^{i(q-\bar{q})X} \rangle_t e^{-i(qx-\bar{q}y)}] \right\}. \quad (76b)$$

The relevant averages are given by

$$\begin{aligned} \langle b_{q\sigma} b_{\bar{q}\bar{\sigma}} e^{-i(q+\bar{q})X} \rangle_t &= \sum_{p, \bar{p}, \mu} \delta_{\bar{p}-p, q+\bar{q}} e^{i(E_p - E_{\bar{p}})t} \langle \omega_p(t) | \omega_{\bar{p}}(t) \rangle \left\{ \frac{W_{q\sigma} W_{\bar{q}\bar{\sigma}}}{4L} [(c_{p\mu} a_{p\mu})^* c_{\bar{p}\mu} a_{\bar{p}\mu} \chi_t(\Omega_{q\sigma}(\bar{p})) \chi_t(\Omega_{\bar{q}\bar{\sigma}}(\bar{p})) \right. \\ &\quad \left. + \sigma e^{-i\mu 2J_\perp t} (c_{p\mu} a_{p\mu})^* c_{\bar{p}\mu} a_{\bar{p}\mu} (\chi_t(\Omega_{q\sigma}^{-\mu}(\bar{p})) \chi_t(\Omega_{\bar{q}\bar{\sigma}}(\bar{p})) - \chi_t(\Omega_{q\sigma}(\bar{p})) \chi_t(\Omega_{\bar{q}\bar{\sigma}}^{-\mu}(\bar{p}))) \right] \\ &\quad \left. + 2(c_{p\mu} a_{p\mu})^* [c_{\bar{p}\mu} a_{\bar{p}\mu} A_{q\sigma, \bar{q}\bar{\sigma}}^{\mu\mu}(\bar{p}, t) + c_{\bar{p}\mu} a_{\bar{p}\mu} A_{q\sigma, \bar{q}\bar{\sigma}}^{\bar{\mu}\bar{\mu}}(\bar{p}, t)] \right\} + \mathcal{O}((gK^{1/2}/v)^3) \end{aligned} \quad (77a)$$

$$\begin{aligned} \text{and } \langle b_{q\sigma}^\dagger b_{\bar{q}\bar{\sigma}} e^{i(q-\bar{q})X} \rangle_t &= \frac{W_{q\sigma} W_{\bar{q}\bar{\sigma}}}{4L} \sum_{p, \bar{p}, \mu} \delta_{\bar{p}-p, -q+\bar{q}} e^{i(E_p - E_{\bar{p}})t} \langle \omega_p(t) | \omega_{\bar{p}}(t) \rangle [(c_{p\mu} a_{p\mu})^* c_{\bar{p}\mu} a_{\bar{p}\mu} (\chi_t^*(\Omega_{q\sigma}(p)) \chi_t(\Omega_{\bar{q}\bar{\sigma}}(\bar{p})) \\ &\quad - \chi_t^*(\Omega_{q\sigma}^{+\mu}(p)) \chi_t(\Omega_{\bar{q}\bar{\sigma}}^{+\mu}(\bar{p}))) + \sigma e^{-i\mu 2J_\perp t} (c_{p\mu} a_{p\mu})^* c_{\bar{p}\mu} a_{\bar{p}\mu} \\ &\quad \times (\chi_t^*(\Omega_{q\sigma}^{+\mu}(p)) \chi_t(\Omega_{\bar{q}\bar{\sigma}}(\bar{p})) - \chi_t^*(\Omega_{q\sigma}(p)) \chi_t(\Omega_{\bar{q}\bar{\sigma}}^{-\mu}(\bar{p})))] + \mathcal{O}((gK^{1/2}/v)^3). \end{aligned} \quad (77b)$$

We point out that, although the results presented thus far are nonperturbative in J_\perp , there are observables for which the limit $J_\perp \rightarrow 0$ can be problematic. The simple density averages (73) show the correct physical behavior for vanishing J_\perp , namely that if the impurity is initialized in one of the baths at $J_\perp = 0$, only the densities of this bath will develop a nonzero average during the time evolution, while the averages for the other bath will remain rigorously zero. Analogously, also the impurity averages have a physically sound $J_\perp \rightarrow 0$ limit.

On the other hand, for the interbath correlation functions we run into a problem. In the limit $J_\perp \rightarrow 0$ the baths become decoupled, therefore we expect $\langle \rho_\sigma(x) \rho_{\bar{\sigma}}(y) \rangle_t |_{J_\perp=0} = \langle \rho_\sigma(x) \rangle_t |_{J_\perp=0} \langle \rho_{\bar{\sigma}}(y) \rangle_t |_{J_\perp=0}$ (and analogously for momentum). However, this property is not satisfied by the perturbative expressions given above. This violation comes about because in our perturbative solution we broke up the interaction in two terms, treating one exactly (inraband processes) while expanding in the second one (interband processes). When $J_\perp = 0$, this separation is not justified, and it actually gives rise to a spurious residual interbath correlation. This appears to be a limitation of our perturbative approach. Nevertheless, the unphysical $J_\perp = 0$ contribution is small, and so we believe that the interbath correlation functions that we compute still contain useful physical information about the system and its evolution. To be sure to avoid showing unphysical features in the correlation functions, in the next section we will show them with their small spurious $J_\perp = 0$ values subtracted.

VI. NUMERICAL RESULTS

In this section, we show numerical results for the evolution of the impurity probability density, the bath density, and bath momentum density when the impurity is initialized in a wave packet within the \uparrow bath ($\sigma = 1$). The method we

employed allows for virtually arbitrary wave packets, compatibly with the low-momentum conditions for the validity of the long-wavelength model. We choose a Gaussian profile in momentum space

$$c_{p\mu} = 2^{-1/2} N(p_0, \delta p) e^{-\frac{(p-p_0)^2}{4\delta p^2} - ix_0 p}, \quad (78)$$

where p_0 is the average momentum, δp is the width of the distribution, x_0 is the average initial position, and $N(p_0, \delta p)$ is chosen to ensure that $\sum_{p\mu} |c_{p\mu}|^2 = 1$. Notice that the above momentum profile corresponds to a wave function that is factorized between space and bath indices. This choice is not required by our perturbative method, but it simplifies the analysis of the results. We work in a finite-size system of length L , with periodic boundary conditions. Momenta are then quantized according to $p_n = 2\pi/L \cdot n$, $n \in \mathbb{Z}$, and we take a wave packet composed of N_p momenta, distributed symmetrically around p_0 [34]. We usually take $N_p = 32$ or $N_p = 64$ momenta, and $x_0 = L/2$. We always consider $L = 1000(Mv)^{-1}$. We measure momenta, lengths, and energies respectively in units of Mv , $(Mv)^{-1}$, and Mv^2 , namely we take $M = 1$ and $v = 1$ (along with $\hbar = 1$). The baths start always in their ground states.

A. Impurity oscillations

In Figs. 4(a) and 4(b) we show the time evolution of $\langle n_\uparrow \rangle_t$, namely the probability of finding the impurity in bath \uparrow at time t (the probability for the other bath is simply $\langle n_\downarrow \rangle_t = 1 - \langle n_\uparrow \rangle_t$). We can observe that the interaction with the baths has two effects. First, the amplitude of the oscillations around the average value $1/2$ becomes a decreasing function of time. This decay is more pronounced for larger coupling [Fig. 4(b)] and larger J_\perp [Fig. 4(a), once the time is measured in J_\perp -independent units]. Second, the frequency of the oscillations

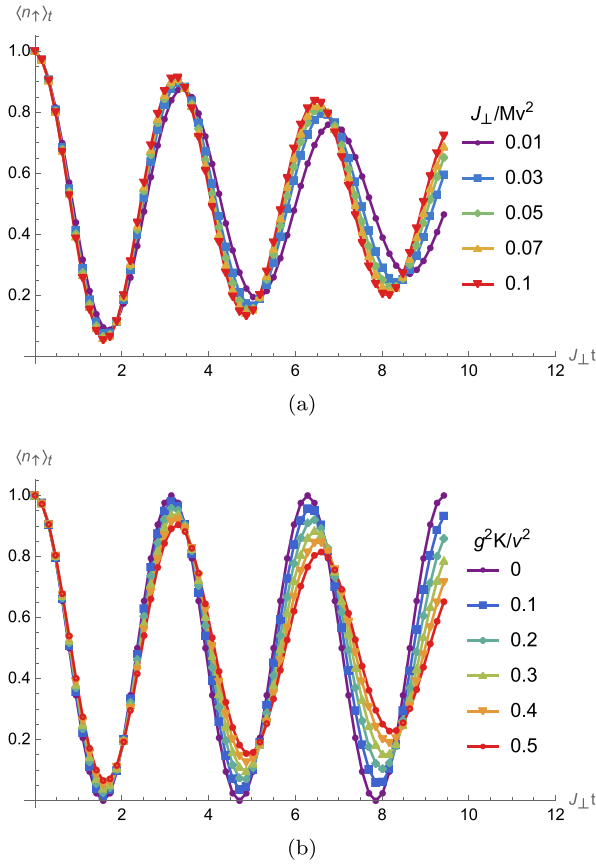


FIG. 4. Time evolution of $\langle n_{\uparrow} \rangle$ for the wave packet Eq. (78). In plot (a) the coupling is kept fixed to $g^2 K = 0.5v^2$, while J_{\perp} is varied, while in plot (b) we vary the coupling while keeping a constant $J_{\perp} = 0.05Mv^2$. Notice that in both plots the time is expressed in units of J_{\perp}^{-1} , which means that in (a) the time unit is different for different plots.

is decreased, by an amount that is larger for increasing coupling [Fig. 4(b)] and decreasing J_{\perp} [Fig. 4(a)].

We can have an analytic insight on these observations by examining the expression (65) for $\langle n_{\uparrow} \rangle_t$. In particular, if we keep only the first term in the bath states overlap (66), which gives the leading contribution, and we use the asymptotic relations Eqs. (61) for $a_{p\mu}$, we find

$$\langle n_{\sigma} \rangle_t \sim \frac{1}{2} + \sigma \Re \sum_p e^{z_{pe}^* + z_{po}} c_{pe}^* c_{po} e^{-2i\tilde{J}_{\perp,p}t - 2\gamma_p t}, \quad (79)$$

where $\tilde{J}_{\perp,p} \equiv J_{\perp} + (\Delta\lambda_{po} - \Delta\lambda_{pe})/2$ is a renormalized interbath hopping amplitude (see Appendix B). From the above expression we can see that $\langle n_{\sigma} \rangle_t - 1/2$ is a superposition of damped oscillatory functions, one for each momentum in the wave packet. For comparison, in the noninteracting case we would have

$$\langle n_{\sigma} \rangle_t^{(0)} = \frac{1}{2} + \sigma \Re \sum_p c_{pe}^* c_{po} e^{-2iJ_{\perp}t}, \quad (80)$$

which describes the impurity periodically hopping from one bath to the other. In the weak-coupling regime we are examining, the interaction with the baths decreases the hopping frequency ($\tilde{J}_{\perp,p} < J_{\perp}$), while the amplitude of the oscillations

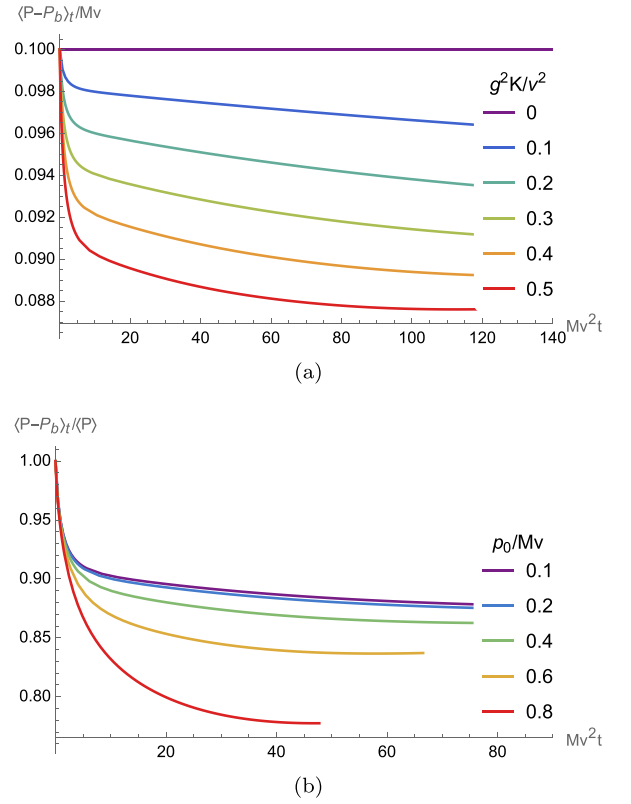


FIG. 5. Time evolution of the impurity momentum for the initial state $|p_0 \uparrow\rangle_d$, and symmetric baths. Plot (a) has $p_0 = 0.1Mv$, $J_{\perp} = 0.05Mv^2$ and shows the effect of increasing the coupling. Plot (b) is for $g^2 K = 0.5v^2$, $J_{\perp} = 0.05Mv^2$ and shows the relative decrease of momentum $\langle P_d \rangle_t / p_0$ for increasing p_0 . In the latter plot, the two curves at higher momentum are limited within the time domain in which where the loss of the state norm does not give rise to spurious effects.

decreases exponentially with a decay time of $1/(2\gamma_p)$. For completeness, we report here the expression of $2\gamma_p$,

$$2\gamma_p = \frac{M}{16\pi} \sum_{\sigma, s=\pm 1} g_{\sigma}^2 K_{\sigma} \left\{ 1 - \left[1 + \frac{4J_{\perp}M}{(Mv_{\sigma} + sp)^2} \right]^{-1/2} \right\}.$$

This decay rate is a monotonically increasing function of both J_{\perp} and p , that vanishes at $J_{\perp} = 0$ because conservation of momentum and energy forbid an impurity moving in 1D from emitting phonons.

While our solution ceases to be accurate beyond the decay time $1/(2\gamma_p)$, it hints at $\langle n_{\sigma} \rangle_t \rightarrow 1/2$ eventually. This limit is what we would expect intuitively as a result of dephasing and dissipation.

B. Impurity momentum

The time evolution of the impurity momentum is displayed in Fig. 5, as function of the various parameters of the model. In all plots, the impurity is initialized in the \uparrow bath with a definite momentum [35] p_0 . We observe that the momentum decay can be divided in two phases: an initial abrupt drop followed by a decrease at a milder rate. Figure 3 shows the effect of the interbath hopping on the momentum. We can see that

the initial rapid decrease is basically unaffected by J_{\perp} , while the subsequent decay is faster for larger hopping. This difference suggests that the two phases of the decay originate from two different processes. We interpret the two phases of momentum decay in the following way: The first fast-decreasing region is caused by the baths relaxing to the injection of the impurity, while in the second phase the impurity momentum is carried away by the phonons generated from the deexcitation of the odd mode.

Indeed, this first phase occurs on a timescale that appears to be independent of J_{\perp} , and well before the impurity starts oscillating into the \downarrow bath [36]. Initially, the first and last terms of Eq. (67) contribute equally to the bath momentum. After the initial transient, the background contribution saturates to a constant value, while the first term of Eq. (67) continues to grow, albeit at a slower rate (except for the unphysical decrease at late times). The timescale of this growth is shorter the larger is J_{\perp} , which is what we expect from the property that the odd-mode decay constant $2\gamma_p$ is an increasing function of J_{\perp} . At the lowest interbath hopping we considered, $J_{\perp} = 0.01Mv^2$, the timescale is so long that the contribution to $\langle P_b \rangle_t$ from the odd-mode decay appears to converge to a value slightly below that of the background.

The dependence of the impurity momentum on the coupling is shown in Fig. 5(a). As expected, the decrease is more marked for stronger coupling, while the two-phase structure is kept unaltered. A larger $gK^{1/2}/v$ increases the fraction of momentum that is lost in the initial transient, but not the timescale in which it occurs.

The following Fig. 5(b) shows the slowdown of the impurity momentum at increasing values of the initial momentum p_0 , as a fraction of the latter. We can recognize the initial transient and the subsequent slower decay, with the former following a common shape for all momenta at small times. After the transient, we see that for increasing p_0 the relative amount of momentum that is transferred to the baths becomes larger, which also translates to a larger absolute decrease of the impurity momentum. This more pronounced decrease for faster impurities may be also traced back to the increase of the decay rate $2\gamma_{p_0}$ with p_0 , which implies that the production of phonons caused by the deexcitation of the odd mode occurs earlier and more rapidly. At smaller momenta $|p| \lesssim 0.2Mv$ the ratio $\langle P_d \rangle_t / p_0$ tends to a common profile, independent of p_0 . This property is explained by noticing that $R_1^{\sigma}(\varepsilon; p_0)$ is linear in p_0 for small momentum $|p_0| \ll Mv_{\sigma}$, hence for a single momentum component $\langle P_b \rangle(t) = v(t)p_0/(Mv) + \mathcal{O}(p_0^2/(Mv)^2)$, with $v(t)$ independent of p_0 .

We briefly comment on the property that the impurity momentum decays monotonically in time. This is in accord with the physical intuition that the impurity is experiencing some kind of (nonclassical) friction as it radiates away its initial kinetic and “internal” energy ($2J_{\perp}$) in the form of phonons. There are at least two reasons for this behavior. Firstly, this occurs because of a cancellation between the momenta acquired by each of the baths. Indeed, the bath momentum Eq. (67) can be decomposed as $\langle P_b \rangle_t = \langle P_b^{\uparrow} \rangle_t + \langle P_b^{\downarrow} \rangle_t$, and the individual contributions from the two baths oscillate out of phase around an average, monotonically increasing value as the impurity swings from one bath to the other. However, when the baths are identical, the oscillations cancel out and a

monotonic function is obtained (if the baths are not identical, there are residual oscillations). The second reason for the monotonic behavior is that we neglected backscattering for the bath particles in the interaction with the impurity. This excludes the appearance of nonmonotonic behavior due to large-momentum exchange (of the order of $2k_F$), as Bloch-like oscillations [12,37].

It can be also observed that the impurity momentum never changes sign during the evolution. While the absence of such a process of impurity backscattering can be expected from physical intuition, it is not forbidden by the interaction Hamiltonian. Indeed, kinematics shows that the decay of the odd mode can be accompanied by the emission of phonons with momenta that can be larger than the initial impurity momentum if J_{\perp} is large enough [38]. The reason why these phonons do not impart such a substantial momentum to the impurity is that they are emitted randomly both in the forward and in the backward direction with respect to the impurity motion [compare with the interaction term in (19)], so that there is an overall compensation to the observed small value.

C. Impurity density evolution

The typical time evolution of the probability density of the impurity is reported in Fig. 6(b), compared with the free evolution 6(a). Varying J_{\perp} and g_{σ} produces analogous results. The motion is qualitatively similar to the free one, namely the whole wave packet moves to the right at a speed slightly less than p_0/M while oscillating with a frequency renormalized by the interactions as compared to the noninteracting value $\tilde{J}_{\perp p}$ [see Eq. (B14)]. In the perturbative regime the absolute effect of the baths on the impurity momentum and frequency of oscillation is typically small.

A visible difference between the free and interacting time evolution of the wave packet is the larger spread of each peak in the “time direction”, which means that the impurity never really leaves any of the baths for the other [39]. This phenomenon can be traced back to the inhomogeneous dephasing associated to the momentum dependence of the renormalized interbath hopping $\tilde{J}_{\perp p}$. The increased spread in the time direction can be interpreted as the initial evidence of the decay of the odd mode, which implies that eventually any oscillation should disappear.

There is also a second difference between the interacting and the free-density evolution, namely the enhanced rate of decrease of the height of the wave packet. This decrease arises partly from the progressive loss of the norm of the state, and partly from the rapid flowing of probability towards the tails of the distribution. While this could signal an actual tendency of the impurity to spread, we suspect that this behavior is an artifact induced by the perturbative method. On the other hand, the shape of the packet around its center remains Gaussian with good approximation.

D. Bath density evolution

We have already presented an overview of the evolution of the density of the baths in Sec. III. In the following paragraphs, we will provide more details.

In Fig. 7 we show the bath density evolution for increasing values of J_{\perp} , keeping all other parameters constant. The

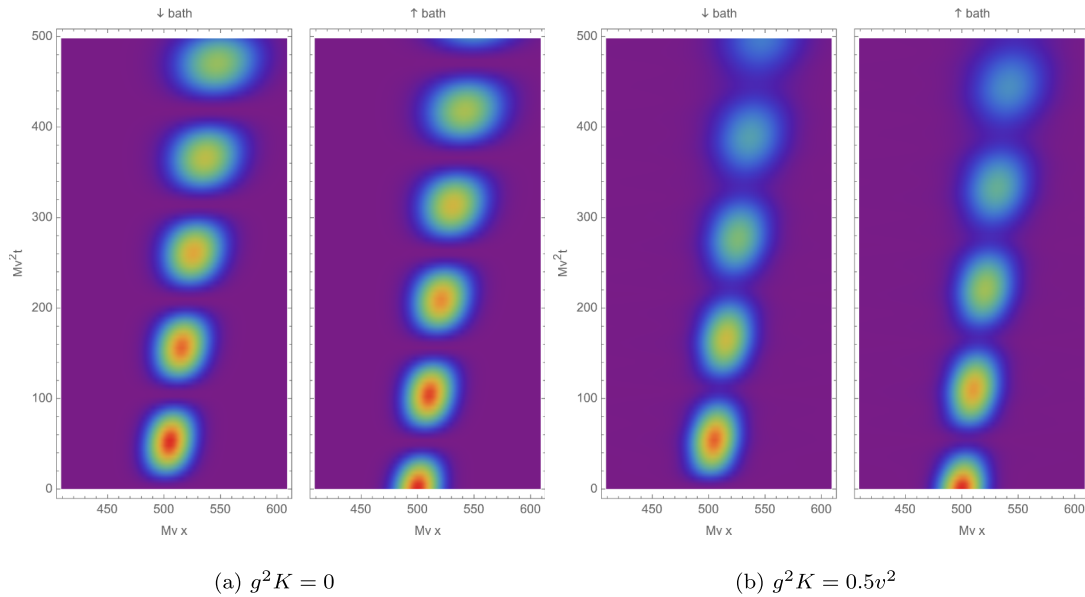


FIG. 6. Comparison of the time evolution of probability density for (a) the free and (b) the interacting impurity with symmetric baths, $g^2 K = 0.5v^2$ and $J_{\perp} = 0.03Mv^2$. In both figures the wave packet is initialized with the Gaussian distribution Eq. (78) of $N_p = 64$ momenta around $p_0 = 0.1Mv$, with standard deviation $\delta p = 0.04Mv$. The total length of the system is $L = 1000(Mv)^{-1}$, but only its central part is depicted. The normalization of the color scale for the two figures is the same.

baths have identical properties. The initial impurity wave packet starts in the \uparrow bath, with an average position $x_0 = L/2$ and a momentum distribution of $N_p = 64$ momenta that are centered around $p_0 = 0.1Mv$, with a width of $\delta p = 0.04Mv$ [correspondingly, the spatial width of the wave packet is about [40] $\delta x \approx 1/(2\delta p) = 12.5(Mv)^{-1}$]. These figures show that the density evolution has a common structure: a depletion that follows the impurity (notice how it is inclined to the right, owing to the nonzero average momentum p_0), flanked by two wave fronts that “radiate” in opposite directions at the speed of sound (which is $v = 1$ in our units). As time goes on, the region between these features (the “light-cone” $|x| \leq vt$) becomes filled with density ripples, which can be interpreted as a manifestation of the emission of real phonons caused by the deexcitation from the odd to the even mode. This interpretation follows from the observation that these ripples ultimately come from the $b_{q\sigma}^{\dagger}|\omega_p(t)\rangle$ terms [i.e., from the last term of Eq. (74)], which we identified as representing spontaneous emission. On the other hand, the depletion and the wave front are all contained in the coherent states $|\omega_p(t)\rangle$. More physically, the ripples have a wavelength that diminishes with increasing J_{\perp} , corresponding to the wave vectors $q_{\pm}(p_0)$ that solve $\Omega_{q_{\pm}\sigma}(p_0) = 2J_{\perp}$. The negative and positive solutions of the latter equation apply to backward and forward emission, respectively, and are Doppler-shifted $q_+(p_0) > |q_-(p_0)|$ because of the motion of the source (the impurity). These observations support our view of the perturbative solution as being decomposed into a “bath relaxation” (depletion and wave fronts) and spontaneous emission.

As J_{\perp} becomes smaller, the ripples become higher and of longer wavelength, and the whole density profile becomes wider. At the same time, the depth of the minimum oscillates more and more evidently, as the impurity oscillation becomes slower. This behavior is consistent with the single-bath

situation that is recovered for $J_{\perp} \rightarrow 0$, in which the impurity remains in its initial bath.

The baths are identical in their properties and initial state, the only source of asymmetry is the initial state of the impurity. The latter causes the \downarrow bath to interact with the impurity a little later than the \uparrow bath (roughly after a fraction of the bare oscillation period $2\pi/J_{\perp}$). Because of this, the density profile of the \downarrow bath is qualitatively similar to the \uparrow one, but it is “delayed” by the time it takes the impurity to change its initial bath. This characteristic is shown in Fig. 8(a). At large J_{\perp} , the impurity is rapidly exchanged, and therefore the baths’ density profiles are “synchronized”, almost coinciding with each other, and with very little relative lag. As J_{\perp} is decreased, the oscillations in the depletion depth become wider and wider and thus can be clearly seen to be out of phase, while the wave fronts are always in phase but show a visible lag. Moreover, the wave fronts in the \downarrow bath decrease in height with respect to their \uparrow counterparts when J_{\perp} assumes smaller values. The ripples are rigorously out of phase. In fact, we have already remarked that the ripples come from the second term in the square brackets in Eq. (74), which is multiplied by $\sigma = \pm 1$.

We point out that the depletion and wave fronts have a distinct shape from that of the ripples. This difference is also evident from the observation that the wavelength of the ripples depends on J_{\perp} , whereas the width of the other two does not. Indeed, it is not hard to guess that depletion and wave fronts are essentially “images” of the Gaussian profile of the impurity wave packet, albeit slightly distorted. The shape of the ripples is instead more or less sinusoidal, and this suggests that their behavior is governed by the intrinsic dynamics of the baths, rather than by the details of the shape of the wave packet.

These observations are substantiated by investigating the effect of the initial wave packet width on the bath density profile. This analysis is shown in Fig. 8(b), in which the

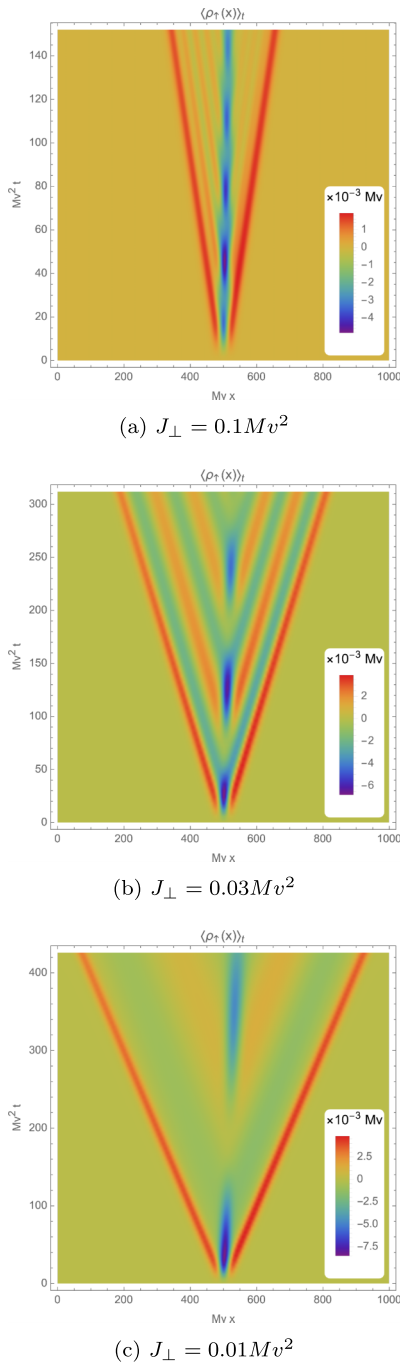


FIG. 7. Dynamics of the density perturbation of bath \uparrow caused by the introduction of an impurity wave packet. The parameters are $g^2 K = 0.5v^2$, $K = 2$ for both baths. The cutoffs are $Mv\alpha = 0.5$ and $\Lambda = 10Mv^2$. Plots (a) to (c) differ in the interbath hopping J_{\perp} .

density profile of the \uparrow bath at a given time is compared for decreasing widths $\delta x \approx 1/(2\delta p)$, at fixed interbath hopping. To keep the wave packet shape unaltered while decreasing its standard deviation, we have kept the ratio $\delta p/N_p$ constant. The main effect of a smaller width is that the magnitude of the density fluctuations is increased. This effect is easily understood for the wave fronts and the central depletion if we trust the observation that they have the same shape as the wave packet, as a narrower normalized Gaussian is also taller. On

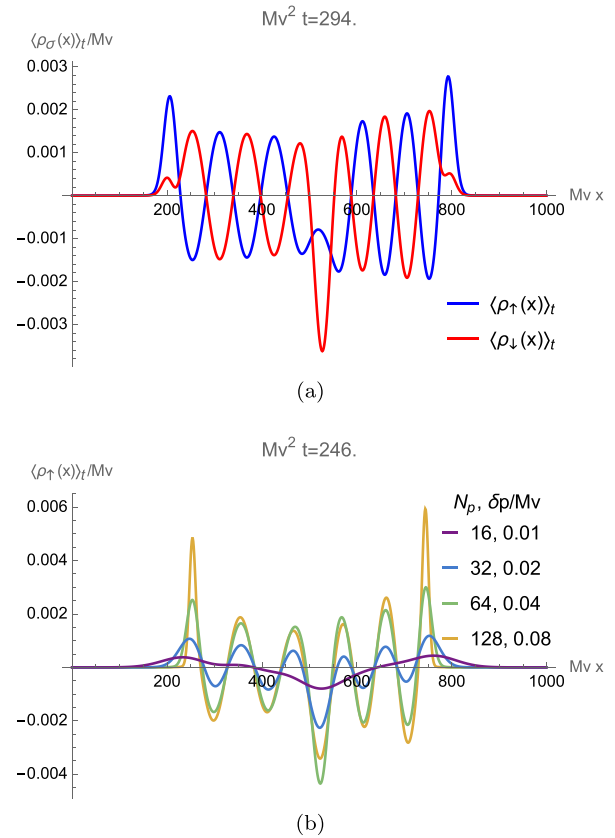


FIG. 8. (a) Density profile in both baths at a given instant of time. (b) Density profile in bath \uparrow for various widths of the wave packet. Both plots are for $J_{\perp} = 0.03Mv^2$, while the other parameters are the same as Fig. 7.

the other hand, the influence on the height of the ripples can be partially understood by observing that wave packets with maximal width (equal to the length of the system) are made of only one momentum, and therefore [compare with Eqs. (73)] produce no density perturbation in the baths. Then, a continuity argument suggests that wider wave packets should give rise to smaller density fluctuations, including the ripples.

We also notice that the dependence of the density fluctuation amplitude is more prominent for the ripples than for the through and wave fronts, to the point that a wide enough wave packet is able to effectively suppress the ripples altogether. Indeed, from Fig. 8(b) we can see that at $J_{\perp} = 0.03Mv^2$ the density perturbation for the wave packet $\delta p = 0.01Mv$ lacks the ripples. We also verified that at $J_{\perp} = 0.1Mv^2$, a standard deviation of $\delta p = 0.02Mv$ is sufficient to cancel the ripples, whereas for $J_{\perp} = 0.01Mv^2$ the ripples are present even for $\delta p = 0.01Mv$. On the other hand, the wavelength of the ripples is not affected by the wave packet width, whereas the central dip and the wave fronts change their shape, becoming narrower and more peaked as δp is increased. This is in accord with our observation that they should be shifted images of the initial wave packet.

In Appendix E we show that the behavior of the ripples amplitude (i.e., their suppression for sufficiently large J_{\perp} or small δx) can be explained as an interference effect, in which there is a cancellation between opposite-sign terms at different

times in the past. This destructive interference occurs only if the initial wave packet is wide enough, according to the relation

$$\delta x \gtrsim \delta x_{c,\sigma}^{\pm}(p_0, J_{\perp}),$$

$$\delta x_{c,\sigma}^{\pm}(p_0, J_{\perp}) \equiv \left(v_{\sigma} \pm \frac{p_0}{M} \right) \frac{\pi}{2\tilde{J}_{\perp,p_0}}. \quad (81)$$

Equivalently, the ripples are suppressed if the momentum distribution is sufficiently narrow,

$$\delta p \lesssim \delta p_{c,\sigma}^{\pm}(p_0, J_{\perp}),$$

$$\delta p_{c,\sigma}^{\pm}(p_0, J_{\perp}) \equiv \frac{\tilde{J}_{\perp,p_0}}{\pi \left(v_{\sigma} \pm \frac{p_0}{M} \right)}. \quad (82)$$

Ignoring for a moment the dependence on p_0 , we see that $\delta p_{c,\sigma}^{\pm}(p_0, J_{\perp})$ is about $0.03Mv$ for $J_{\perp} = 0.1Mv^2$ and $0.01Mv$ for $J_{\perp} = 0.03Mv^2$. So, we see that the above inequalities are indeed satisfied in the above-mentioned cases in which there were no ripples. The positive or negative sign in Eqs. (81) and (82) refer to the ripples emitted backward or forward, respectively. This directional dependence allows us to justify the asymmetric height of the ripples, as the critical width for backward emission is larger than the one for the forward emission, which implies that the cancellation effect is less effective in the backward direction, resulting in the larger ripple amplitude that we observed.

We have also computed the momentum density $\langle \Pi_{\sigma}(x) \rangle_t$, and two examples are shown in Fig. 9. The time evolution of the momentum density shares many qualitative features with the density. There is a central part that follows the motion of the impurity, made of a relative minimum and a maximum that oscillate in time, cyclically exchanging their roles. From them, two trains of ripples expand in opposite directions, up to two wave fronts. Contrary to the density, these wave fronts are out of phase: the left-moving one is positive, while the right-moving one is negative. This property does not seem to be related to the sign of the momenta in the wave packet. As in the case of the density, the central part and the wave fronts are always present for any J_{\perp} , whereas the ripples increase their amplitude as J_{\perp} becomes smaller. Moreover, all features except from the wave fronts are out of phase between the two baths.

We want to briefly comment upon the scaling of the densities with Luttinger parameters K_{σ} . In the long-wavelength effective Hamiltonian (11), K_{σ} enters only through the combination $\tilde{g}_{\sigma} \equiv g_{\sigma} K_{\sigma}^{1/2}$, hence the expectation value Eq. (74) of $\langle e^{-iqX} b_{q\sigma} \rangle$ only depends on \tilde{g}_{σ} . On the other hand, the densities Eqs. (73) explicitly contain K_{σ} , and we can express their scaling as

$$\langle \rho_{\sigma}(x) \rangle_t = K_{\sigma}^{1/2} f_{\rho}(g_{\uparrow}^2 K_{\uparrow}, g_{\downarrow}^2 K_{\downarrow}), \quad (83a)$$

$$\langle \Pi_{\sigma}(x) \rangle_t = K_{\sigma}^{-1/2} f_{\Pi}(g_{\uparrow}^2 K_{\uparrow}, g_{\downarrow}^2 K_{\downarrow}), \quad (83b)$$

where f_{ρ} and f_{Π} are two appropriate functions that we do not need to specify here. From the equations above, we can deduce that the *shape* of the density profiles is controlled only by the effective coupling \tilde{g}_{σ} , while if one varies K_{σ} while keeping $\tilde{g}_{\sigma} = g_{\sigma} K_{\sigma}^{1/2}$ fixed the density or momentum profile

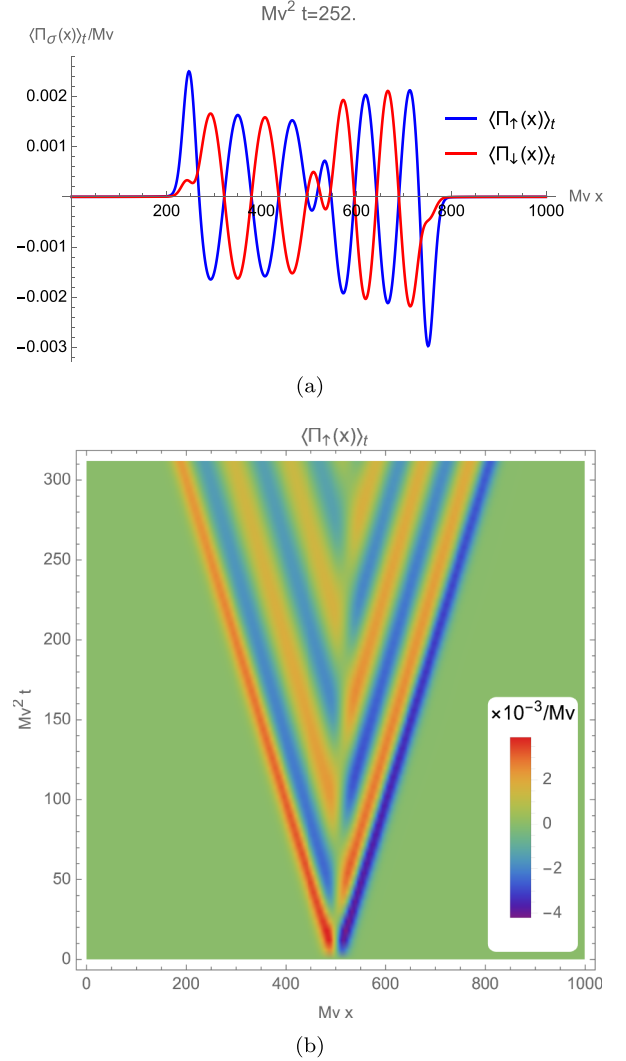


FIG. 9. Momentum density evolution. Plot (a) shows a snapshot of the momentum density profiles for both baths, while (b) shows the full evolution of the \uparrow bath momentum density. The wave packet is Gaussian [Eq. (78)], with $N_p = 64$ momenta distributed around $p_0 = 0.1Mv$ with a standard deviation $\delta p = 0.04Mv$. The parameter settings are $g^2 K = 0.5v^2$, $K = 2$ for both baths, and $J_{\perp} = 0.03Mv^2$.

only gets rescaled. Thus, each of the figures shown above can be taken to represent a family of density profiles.

E. Correlation functions

The typical behavior of the equal-time correlation function $\langle \rho_{\uparrow}(x) \rho_{\downarrow}(y) \rangle_t^c$ is shown in Figs. 10–12, for the same initial conditions as in the discussion of the density evolution. All plots refer to the same g_{σ} , while we vary J_{\perp} .

Figures 10(a) and 10(b) show a sequence of “snapshots” of the full spatial behavior of the correlation function at various moments of time. These show that the correlations are concentrated within two “lobes”, with a series of ripples between them. As time advances, the lobes move apart from each other, while both their amplitude and spatial width increase. The expansion is roughly ballistic, that is, all distances increase linearly in time, albeit with a larger speed in the relative

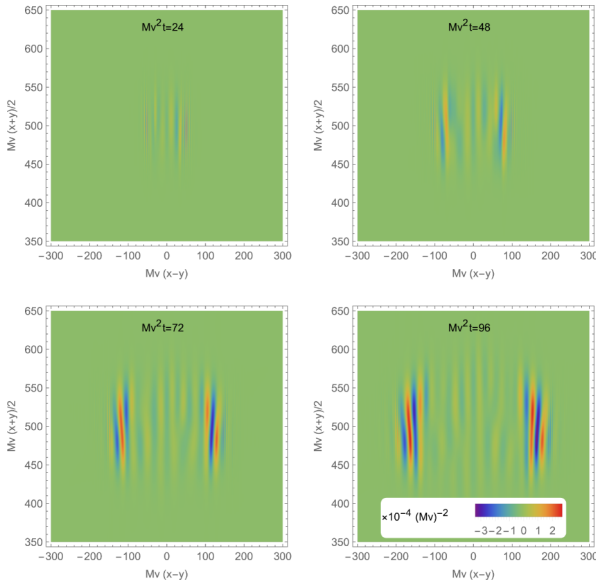
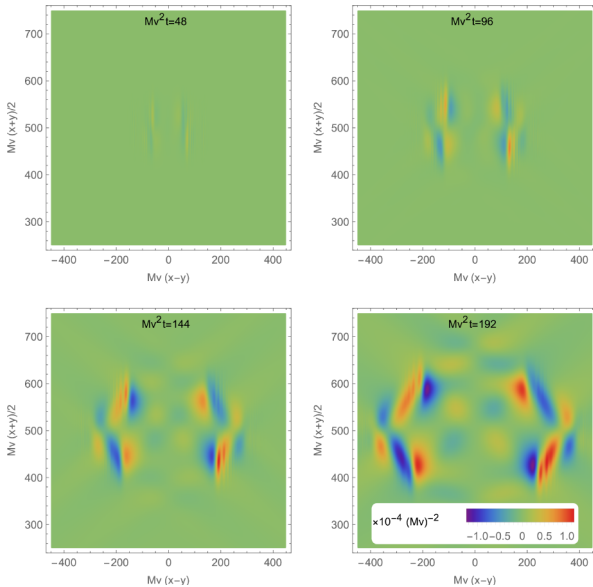
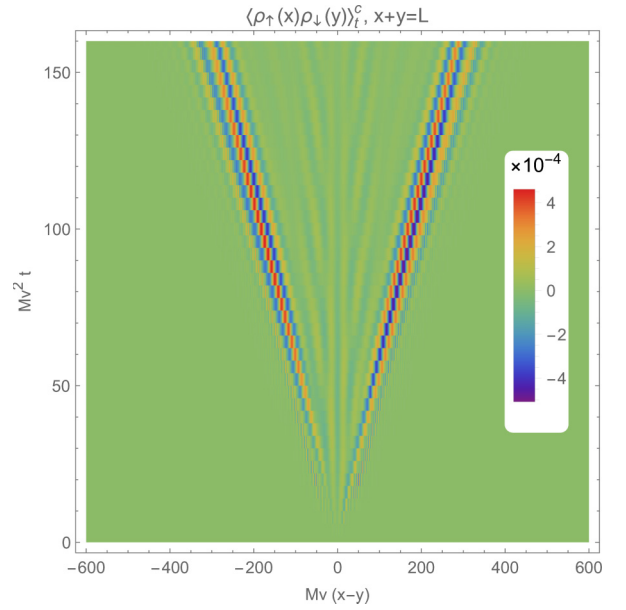

 (a) $J_{\perp} = 0.1 M v^2$

 (b) $J_{\perp} = 0.01 M v^2$

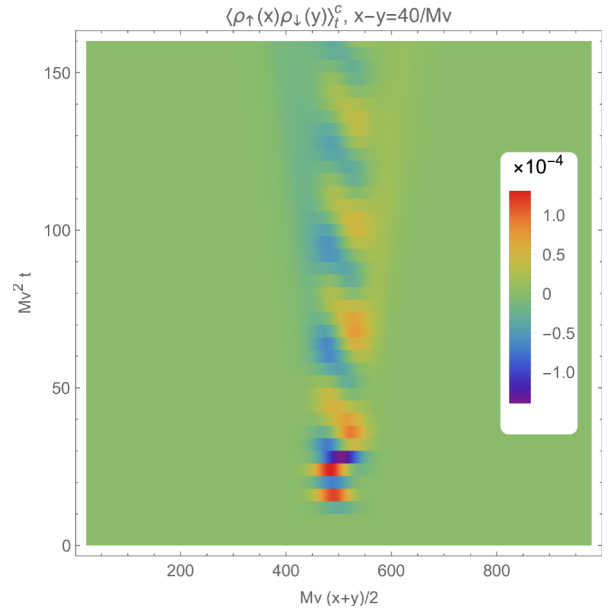
FIG. 10. Time evolution of the connected density-density correlation function $\langle \rho_{\uparrow}(x) \rho_{\downarrow}(y) \rangle_t^c$. The baths are identical, with parameters $g^2 K = 0.5 v^2$ and $K = 2$. The wave packet is Gaussian [Eq. (78)], with $N_p = 32$, $\delta p = 0.02 M v$ and $p_0 = 0.1 M v$. The color scale is normalized to the last “snapshot” of each set of plots.

$r = x - y$ direction than in the “center-of-mass” $R = (x + y)/2$ one. As this expansion takes place, in the region between the lobes a series of ripples form and increase their amplitude in time.

We remark that we have stopped all calculations before the light cone gets too close to the edges of the system [41], in order to avoid finite-size effects (besides the discretization of momenta). Therefore, the observed features should be a result of the intrinsic dynamics of the system under investigation, rather than an effect of interference through the boundaries.



(a)



(b)

FIG. 11. Two “slices” of the density correlation function evolution at $J_{\perp} = 0.1 M v^2$ [the same shown in Fig. 10(a)]. The parameters are the same as Fig. 10. Figure (a) shows it as a function of the relative coordinate $r = x - y$, while (b) uses the center of mass coordinate $R = (x + y)/2$.

These interbath density (or momentum) correlation functions are not symmetric under exchange of x and y , even though $\rho_{\uparrow}(x)$ [or $\Pi_{\uparrow}(x)$] and $\rho_{\downarrow}(y)$ [$\Pi_{\downarrow}(y)$] commute and that the baths have identical properties. The asymmetry arises because the evolution is made asymmetric by the initial conditions, namely the impurity starting in bath \uparrow , with an average nonzero momentum. However, from Fig. 10 it is easy to notice an approximate anti-symmetry with respect to the lines $r = 0$ and $R = L/2$.

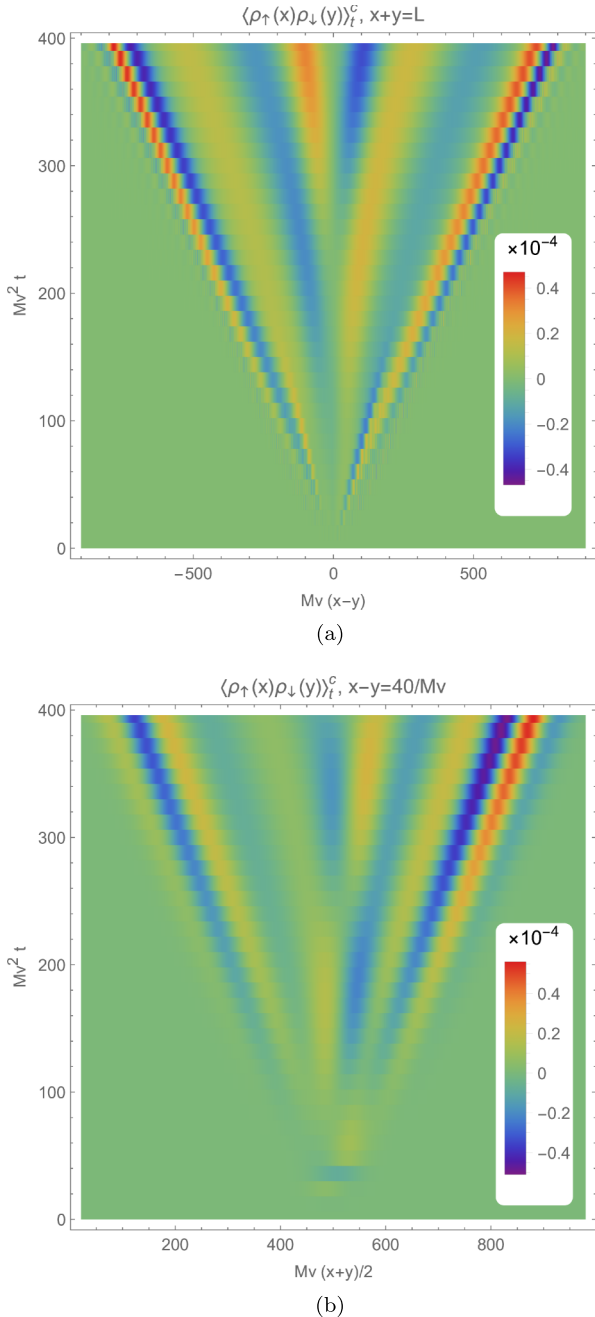


FIG. 12. Two “slices” of the density correlation function evolution at $J_{\perp} = 0.01Mv^2$ [the same shown in Fig. 10(b)]. The parameters are the same as Fig. 10. Figure (a) shows it as a function of the relative coordinate $r = x - y$, while (b) uses the center of mass coordinate $R = (x + y)/2$.

Analogously to the case of the density averages, the correlation functions obey a specific scaling with respect to the Luttinger parameters K_{σ} ,

$$\langle \rho_{\uparrow}(x)\rho_{\downarrow}(y) \rangle_t = (K_{\uparrow}K_{\downarrow})^{1/2} f_{\rho\rho}(g_{\uparrow}^2 K_{\uparrow}, g_{\downarrow}^2 K_{\downarrow}), \quad (84a)$$

$$\langle \Pi_{\uparrow}(x)\Pi_{\downarrow}(y) \rangle_t = (K_{\uparrow}K_{\downarrow})^{-1/2} f_{\Pi\Pi}(g_{\uparrow}^2 K_{\uparrow}, g_{\downarrow}^2 K_{\downarrow}). \quad (84b)$$

The scaling of the densities, Eq. (83), ensures that the same relation holds for the connected correlation functions. We have verified numerically that changing $g_{\sigma}K_{\sigma}^{1/2}$ only causes

minor changes in the shape of the correlation functions, apart from an obvious change in the amplitude. The most relevant shape modifications are those induced by a change in J_{\perp} . At large J_{\perp} [Fig. 10(a)], the correlation function oscillates basically only in the relative r direction, whereas the profile along R shows less features. As J_{\perp} is lowered [Fig. 10(b)], the shape of the lobes becomes more complex, mainly because the correlation function oscillates also in the R direction. Moreover, the ripples “leak out” of the interlobe region.

In the next figures we consider the behavior as a function of, respectively, the relative coordinate $r = x - y$ and center-of-mass coordinate $R = (x + y)/2$.

In the time evolution of $\langle \rho_{\uparrow}(x)\rho_{\downarrow}(y) \rangle_t^c$ as a function of the coordinate difference, as shown in Figs. 11(a) and 12(a), correlations appear only within a “light-cone” $|x - y| \leq vt$. The maximal amplitude occurs around the light-cone itself ($|x - y| \approx vt$), while within the interior there are waves that appear to be radiated from $x = y$. A comparison with Fig. 10 leads to identify the light-cone region with the lobes, while the waves in the interior are the ripples. The wavelength of the latter roughly corresponds to that of the phonons emitted during the deexcitation of the odd impurity mode. This identification, as in the case of the density, comes from the analytical expressions [Eqs. (77)], and from the observation that the wavelength is essentially independent of g_{σ} and K_{σ} , while it is inversely correlated with J_{\perp} , as can be appreciated by comparing Fig. 11 and Fig. 12. As in the case of the average densities, the amplitude of these “ripples” increases for smaller J_{\perp} .

Summing up, the behavior of the correlation function along the relative coordinate basically reflects the “relativistic” nature of TLL bath dynamics, namely that interbath correlations are generated and propagated as linearly dispersing sound modes.

The situation looks different in the center-of-mass coordinate R , as Figs. 11(b) and 12(b) show. Here, we can distinguish a central area in which two trains of ripples oscillate out of phase, and an outer area formed of waves that radiate at the speed of sound from the central area. This distinction is sharp for higher J_{\perp} [Fig. 11(b)], as the amplitude of the emitted waves increase with decreasing J_{\perp} . The inner ripples occupy an area that spreads very slowly in space, and is centered along the trajectory $R = L/2 + p_0t/M$. Moreover, their oscillations in time occur with a period of about π/J_{\perp} , that is, half of the impurity oscillation period. These clues leads us to identify this “section” of the correlation function as the one more closely reflecting the motion of the impurity and the profile of its wave packet. In order to plot Figs. 11(b) and 12(b), we chose a value for r . Changing it causes two main effects: first, the correlation function is zero up to a time that increases with r (a light-cone effect). Second, as r is decreased the oscillations in time get washed away by a featureless background contribution, until at $r = 0$, i.e., $x = y$, there are no more visible oscillations. For all the parameters we checked, $\langle \rho_{\uparrow}(x)\rho_{\downarrow}(x) \rangle_t^c$ is always negative.

The properties of the correlation functions can be rationalized using Eq. (22). We already noticed that, since this equation is a relation between operators, it implies a whole hierarchy of relations that go beyond linear response theory.

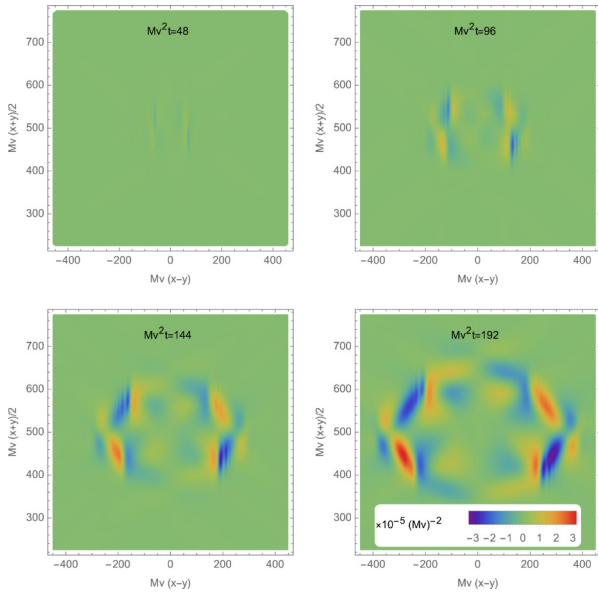


FIG. 13. Time evolution of the connected momentum density correlation function $\langle \Pi_{\uparrow}(x)\Pi_{\downarrow}(y) \rangle_t^c$. The baths are identical, with parameters $g^2K = 0.5v^2$, $K = 2$, and $J_{\perp} = 0.01Mv^2$. The color scale is normalized to the last “snapshot” of each set of plots.

Indeed, we can compute

$$\begin{aligned}
 & \langle \rho_{\sigma}(x)\rho_{\bar{\sigma}}(y) \rangle_t^c \\
 &= g_{\sigma} \int dx_1 dt_1 \chi_{\sigma}(x-x_1, t-t_1) \langle N_{\sigma}(x_1, t_1) \rho_{\bar{\sigma}}(y, 0) \rangle \\
 &+ g_{\bar{\sigma}} \int dx_2 dt_2 \chi_{\bar{\sigma}}(x-x_2, t-t_2) \langle \rho_{\sigma}(x, 0) N_{\bar{\sigma}}(x_2, t_2) \rangle \\
 &+ g_{\uparrow} g_{\downarrow} \int dx_1 dt_1 dx_2 dt_2 \chi_{\sigma}(x-x_1, t-t_1) \\
 &\quad \times \chi_{\bar{\sigma}}(x-x_2, t-t_2) \langle N_{\sigma}(x_1, t_1) N_{\bar{\sigma}}(x_2, t_2) \rangle^c, \quad (85)
 \end{aligned}$$

where we see that the bath density correlation function is related to the connected impurity density correlation function

$$\begin{aligned}
 \langle N_{\sigma}(x_1, t_1) N_{\bar{\sigma}}(x_2, t_2) \rangle^c &\equiv \langle N_{\sigma}(x_1, t_1) N_{\bar{\sigma}}(x_2, t_2) \rangle \\
 &- \langle N_{\sigma}(x_1, t_1) \rangle \langle N_{\bar{\sigma}}(x_2, t_2) \rangle, \quad (86)
 \end{aligned}$$

which, unlike $\langle \rho_{\sigma}(x)\rho_{\bar{\sigma}}(y) \rangle_t^c$, correlates the impurity density at different times, and so it cannot be calculated from the knowledge of $|\Psi(t)\rangle$ only. Thus, in principle we could use Eq. (85) to compute this impurity density correlation function. For now, we can just point out that thanks to this formula we have a hint on why $\langle \rho_{\sigma}(x)\rho_{\bar{\sigma}}(y) \rangle_t^c$ as a function of $(x+y)/2$ seems to mirror the time evolution of the impurity wave packet—indeed, we can now understand that it is keeping track of the impurity density (and impurity-bath density) correlation function.

We conclude this section by briefly discussing the connected momentum correlation function, $\langle \Pi_{\uparrow}(x)\Pi_{\downarrow}(y) \rangle_t^c$. An example is shown in Fig. 13. It shows the same qualitative features of the density correlation function, namely a pair of expanding lobes enclosing a region of smaller oscillations. The main differences with the density correlation are the more complex pattern of the ripples, and sign of the correlation for

$x = y$, which is positive for the momentum and negative for the density.

VII. CONCLUSIONS

In this paper, we have thoroughly studied an impurity hopping on a ladder whose two legs are described in terms of two Tomonaga-Luttinger liquid baths.

We studied the problem from the perspective of the impurity and of the baths themselves, employing an improved perturbative technique. Albeit *a priori* limited to small couplings, the method we used is rather simple, and has the advantage of providing analytical results for the whole system-bath state. Moreover, it is capable of treating the motion of wave packets with only a modest numerical effort.

A comparison with a more conventional Green’s function method, the linked cluster expansion, showed that, at least in a symmetric setting where the two baths are identical, our perturbative technique yields the same result.

We analyzed the effect of the impurity motion on the bath density (and momentum density), finding that they mirror each other, with a behavior, which reminds the simple picture of a stone thrown in a pond. In each of the baths we observed two wave fronts generated by the insertion of the impurity and propagating away from it (i.e., the “rings” on the water surface in the pond analogy), a central density depletion following the impurity, and the emission of ripples as the impurity oscillates between the baths. The latter, in particular, are interpreted as a visualization of the phonon emission as the impurity loses its internal energy.

Then, we proceeded to examine the correlation between the two baths that is generated as they exchange the impurity. We did this by computing the interbath, connected density and momentum density correlation functions at equal times, unveiling a rich spatial structure. The correlation is nonvanishing only within an area in (x, y) space, which expands ballistically. Two features can be distinguished: a pair of lobes and a series of ripples between them. Along the relative direction, $r = x - y$, the correlation function mainly shows the “relativistic” dynamics of the bath, with a clear light-cone as the phonons generated by the impurity spread the correlations. Along the center-of-mass direction $R = (x + y)/2$, instead, the light-cone of emitted phonons is superimposed with the density perturbation following the impurity wave packet in its motion.

There are various directions in which this paper can be extended. An interesting direction is to explore the regime of stronger coupling between the impurity and the baths. A first step towards this regime would be to include the backscattering term in the interaction, and to see its effect within the perturbative formulation. A different approach would be to promote the perturbative expression of the state, Eq. (60), to a variational Ansatz whose coefficients would have to be found numerically. A second intriguing extension of this paper would be to explore the effect of increasing the number of baths where the impurity can move.

ACKNOWLEDGMENTS

We acknowledge useful discussions with A. Recati and F. Scazza. We acknowledge financial support from MIUR

through the PRIN 2017 Program (Protocol No. 20172H2SC4 005).

APPENDIX A: A DIFFERENT PERSPECTIVE ON SYMMETRIC BATHS

The physics of the system under investigation may be clearer in the case of symmetric baths, i.e., for $v_\sigma = v$, $K_\sigma = K$, and $g_\sigma = g$ (hence, $W_{q\sigma} \equiv W_q$). In this regime, it is useful to introduce even and odd bath modes,

$$b_{q\mu=e/o} \equiv \frac{1}{2^{1/2}}(b_{q\uparrow} \pm b_{q\downarrow}), \quad (\text{A1})$$

and recast Hamiltonian (19) as

$$\begin{aligned} \mathcal{H}_{\text{LLP}}(p) &= \frac{(p - P_e - P_o)^2}{2M} - J_\perp \sigma_1 + \sum_q v|q|b_{qe}^\dagger b_{qe} \\ &+ \sum_q \frac{W_q}{(2L)^{1/2}}(b_{qe} + b_{qe}^\dagger) + \sum_q v|q|b_{qo}^\dagger b_{qo} \\ &+ \sigma_3 \sum_q \frac{W_q}{(2L)^{1/2}}(b_{qo} + b_{qo}^\dagger), \end{aligned} \quad (\text{A2})$$

where

$$P_\mu \equiv \sum_q q b_{q\mu}^\dagger b_{q\mu}. \quad (\text{A3})$$

It can be observed that the even- and odd-bath modes become partially independent of each other. In particular, only the odd-bath modes are coupled to the impurity, and the de-excitation of the odd impurity band will generate odd-bath modes. The even modes “see” the impurity only through the momentum-momentum coupling with the odd modes in the first term (that is, the kinetic energy of the impurity in the laboratory frame). The decoupling would be complete for a static impurity, namely for $M \rightarrow +\infty$.

With this separation in mind, it is natural to attempt a first approximation in which the bath parity modes evolve independently since odd bath modes are generated only by transitions between the even and odd impurity bands, involving a “gap” $2J_\perp$ in energy. This leads to our choice of the perturbative scheme, Eq. (26), that in this language reads

$$\mathcal{H}_{\text{LLP}}(p) = \mathcal{H}_0(p) + \Delta\mathcal{H}(p), \quad (\text{A4a})$$

$$\begin{aligned} \mathcal{H}_0(p) &\equiv E(p) - J_\perp \sigma_1 \\ &+ \sum_q \Omega_q b_{qe}^\dagger b_{qe} + \sum_q \frac{W_q}{(2L)^{1/2}}(b_{qe} + b_{qe}^\dagger) \\ &+ \sum_q \Omega_q b_{qo}^\dagger b_{qo}, \end{aligned} \quad (\text{A4b})$$

$$\begin{aligned} \Delta\mathcal{H}(p) &\equiv \sigma_3 \sum_q \frac{W_q}{(2L)^{1/2}}(b_{qo} + b_{qo}^\dagger) \\ &+ \frac{P_e P_o}{M} + \sum_\mu \frac{P_\mu^2}{2M}. \end{aligned} \quad (\text{A4c})$$

According to this perspective, the perturbative expression Eq. (54) has a simple interpretation. The background coherent state $|\omega_p(t)\rangle$ contains only even bath modes, that are increasingly populated in time. On the other hand, the odd-bath modes may contain only up to two phonons each, as described by the “first-” and “second-order” corrections, proportional to $b_{q\sigma}^\dagger$ and $b_{q\sigma}^\dagger b_{q'\sigma'}$, respectively. The latter also introduces the correlation between even and odd bath modes as dictated by the $P_e P_o/M$ term in the Hamiltonian.

APPENDIX B: NORMALIZATION FACTORS

In this Appendix, we shortly discuss the properties and the computation of the normalization factors, Eq. (47), adapted from [15]. In particular, we often have to compute expressions in the form $\frac{1}{L} \sum_{q \neq 0, \sigma} W_{q\sigma}^2 f(\Omega_{q\sigma})$, for a given function $f(\Omega_{q\sigma})$. These can be conveniently computed by introducing an appropriate density of states $R^S(\varepsilon)$,

$$\frac{1}{L} \sum_{q \neq 0, \sigma} W_{q\sigma}^2 f(\Omega_{q\sigma}) = \int_0^{+\infty} d\varepsilon f(\varepsilon) R^S(\varepsilon), \quad (\text{B1})$$

where $R^S(\varepsilon) \equiv \sum_{q \neq 0, \sigma} \frac{W_{q\sigma}^2}{L} \delta(\varepsilon - \Omega_{q\sigma})$. In the continuum limit $L \rightarrow +\infty$, $R^S(\varepsilon)$ can be calculated exactly, and for subsonic momenta $|p| < Mv_\sigma$ it reads

$$\begin{aligned} R^S(\varepsilon) &= \frac{M}{(2\pi)^2} \theta(\varepsilon) e^{-\varepsilon/\Lambda} \\ &\times \sum_{\sigma, s = \pm 1} g_\sigma^2 K_\sigma \left[1 - \left(1 + \frac{\varepsilon}{k_{s\sigma}(p)} \right)^{-1/2} \right]. \end{aligned} \quad (\text{B2})$$

In the above equation, $\theta(\varepsilon)$ is the Heaviside theta function, $k_{s\sigma}(p)$ is defined as

$$k_{s\sigma}(p) \equiv \frac{(Mv_\sigma + sp)^2}{2M}, \quad s = \pm 1 \quad (\text{B3})$$

and we introduced an energy cutoff Λ instead of a momentum one, for simplicity.

This density of states is analogous to the ones that characterize the bath in the spin-boson or Caldeira-Leggett models [25]. At small energies $\varepsilon \ll Mv_\sigma^2$ they are linear, so that the Tomonaga-Luttinger liquid baths are classified as ohmic,

$$R^S(\varepsilon) = \theta(\varepsilon) \varepsilon \sum_\sigma \beta_\sigma^{\text{sb}}(p) + \mathcal{O}\left(\frac{\varepsilon^2}{M^2 v_\sigma^4}\right), \quad (\text{B4})$$

where

$$\beta_\sigma^{\text{sb}} = \frac{g_\sigma^2 K_\sigma}{2\pi^2 v_\sigma^2} \frac{1 + (p/Mv_\sigma)^2}{(1 - (p/Mv_\sigma)^2)^2} \quad (\text{B5})$$

is the single-bath orthogonality exponent [15,42].

We have worked out a numerically friendly way of computing the exponents in Eq. (47) in a previous paper [15]. Here we quote only the final results,

$$-\sum_{q \neq 0, \sigma} \frac{W_{q\sigma}^2}{4L} \frac{1 - i(\Omega_{q\sigma} \pm 2J_{\perp})t - e^{-i(\Omega_{q\sigma} \pm 2J_{\perp})t}}{(\Omega_{q\sigma} \pm 2J_{\perp})^2} = -\sum_{\sigma} \frac{M\tilde{g}_{\sigma}^2}{(4\pi)^2} \left\{ f(\pm J_{\perp}, t) + \sum_{s=\pm 1} \left[\frac{1}{k_{s\sigma}(p)} \phi_1\left(\frac{\pm 2J_{\perp}}{k_{s\sigma}(p)}\right) - t\phi_2\left(\frac{\pm 2J_{\perp}}{k_{s\sigma}(p)}\right) + ie^{\pm 2iJ_{\perp}t} \int_0^{+\infty} du \frac{e^{-ut}}{(iu \pm 2J_{\perp})^2} \frac{1}{(1 - iu/k_{s\sigma}(p))^{1/2}} \right] \right\} \quad (\text{B6})$$

where

$$f(\pm J_{\perp}, t) = \pi t \pm 2t \text{Si}(2J_{\perp}t) \mp \frac{1 - \cos 2J_{\perp}t}{J_{\perp}} + 2it \left[\ln \frac{2J_{\perp}}{\Lambda e^{-\eta}} + \Re E_1(2iJ_{\perp}t) + \frac{\sin 2J_{\perp}t}{2J_{\perp}t} \right], \quad (\text{B7})$$

$\text{Si}(z)$ and $E_1(z)$ are the sine and exponential integral functions [43], respectively, and we introduced the functions

$$\phi_1(x) = \begin{cases} \frac{1}{2x(1+x)^{3/2}} \left[\pi x - 2i(\sqrt{x+1} + x \operatorname{arcsinh}(\frac{1}{\sqrt{x}})) \right], & x > 0 \\ \frac{i}{|x|(1-|x|)} - \frac{i}{(1-|x|)^{3/2}} \operatorname{arccosh}(\frac{1}{\sqrt{|x|}}), & x < 0 \end{cases},$$

$$\phi_2(x) = \begin{cases} \frac{1}{\sqrt{1+x}} \left[\pi - 2i \operatorname{arcsinh}(\frac{1}{\sqrt{x}}) \right], & x > 0 \\ -\frac{2i}{\sqrt{1-|x|}} \operatorname{arccosh}(\frac{1}{\sqrt{|x|}}), & x < 0 \end{cases}, \quad (\text{B8})$$

in which it is understood that

$$\operatorname{arccosh}(x) = i \arccos x \quad \text{for } |x| < 1. \quad (\text{B9})$$

Analogously,

$$-\sum_{q \neq 0, \sigma} \frac{W_{q\sigma}^2}{4L} \frac{1 - i\Omega_{q\sigma}t - e^{-i\Omega_{q\sigma}t}}{(\Omega_{q\sigma})^2} = -\sum_{\sigma} \frac{M\tilde{g}_{\sigma}^2}{(4\pi)^2} \left\{ f(0, t) - \sum_{s=\pm 1} i \int_0^{+\infty} du \frac{1 - ut - e^{-ut}}{u^2} \frac{1}{(1 - iu/k_{s\sigma}(p))^{1/2}} \right\}, \quad (\text{B10})$$

where

$$f(0, t) = \pi t - 2it \ln \frac{\Lambda t}{e}. \quad (\text{B11})$$

The manipulations done so far allow us to easily derive the asymptotic behavior of the normalization factors,

$$\ln a_{pe} = -\frac{M}{(4\pi)^2} \sum_{\sigma} \left[\frac{1}{J_{\perp}} + i \sum_{s=\pm} \frac{\phi_1(-2J_{\perp}/k_{s\sigma})}{k_{s\sigma}} \right] - i\Delta\lambda_{pe}t + \mathcal{O}(1/t) \quad (\text{B12a})$$

$$\ln a_{po} = -\frac{M}{(4\pi)^2} \sum_{\sigma} \left[-\frac{1}{J_{\perp}} + i \sum_{s=\pm} \frac{\phi_1(2J_{\perp}/k_{s\sigma})}{k_{s\sigma}} \right] - i\Delta\lambda_{po}t - 2\gamma_p t + \mathcal{O}(1/t), \quad (\text{B12b})$$

where

$$\Delta\lambda_{pe} = \frac{M}{8\pi^2} \sum_{\sigma} g_{\sigma}^2 K_{\sigma} \left[\ln \frac{2J_{\perp}}{\Lambda e^{-\eta}} + \sum_{s=\pm 1} \frac{1}{(1 - 2J_{\perp}/k_{s\sigma}(p))^{1/2}} \operatorname{arccosh}\left(\frac{k_{s\sigma}(p)}{2J_{\perp}}\right)^{1/2} \right] \quad (\text{B13a})$$

$$\Delta\lambda_{po} = \frac{M}{8\pi^2} \sum_{\sigma} g_{\sigma}^2 K_{\sigma} \left[\ln \frac{2J_{\perp}}{\Lambda e^{-\eta}} + \sum_{s=\pm 1} \frac{1}{(1 + 2J_{\perp}/k_{s\sigma}(p))^{1/2}} \operatorname{arcsinh}\left(\frac{k_{s\sigma}(p)}{2J_{\perp}}\right)^{1/2} \right] \quad (\text{B13b})$$

$$2\gamma_p = \frac{M}{16\pi} \sum_{\sigma} g_{\sigma}^2 K_{\sigma} \left[1 - \frac{1}{(1 + 2J_{\perp}/k_{s\sigma}(p))^{1/2}} \right]. \quad (\text{B13c})$$

In the equations above, η is the Euler-Mascheroni constant, and the convention Eq. (B9) is assumed once again. Physically, remembering that $a_{p\mu}$ is always multiplied by $e^{-i\lambda_{p\mu}t}$ [see Eqs. (53) and (54)], we see that $\Delta\lambda_{p\mu}$ renormalize the two bands $\lambda_{p\mu}$, lowering them by a cutoff-dependent quantity and slightly altering their curvature. Moreover, the energy difference between the renormalized bands is reduced with respect to the noninteracting value $2J_{\perp}$. This energy difference can be seen as a renormalized

interbath hopping

$$\begin{aligned} 2\tilde{J}_{\perp p} &\equiv 2J_{\perp} + \Delta\lambda_{po} - \Delta\lambda_{pe} \\ &= 2J_{\perp} - \frac{M}{8\pi^2} \sum_{\sigma, s=\pm 1} g_{\sigma}^2 K_{\sigma} \left[\frac{1}{(1 - 2J_{\perp}/k_{s\sigma}(p))^{1/2}} \operatorname{arccosh} \left(\frac{k_{s\sigma}(p)}{2J_{\perp}} \right)^{1/2} - \frac{1}{(1 + 2J_{\perp}/k_{s\sigma}(p))^{1/2}} \operatorname{arcsinh} \left(\frac{k_{s\sigma}(p)}{2J_{\perp}} \right)^{1/2} \right] \end{aligned} \quad (\text{B14})$$

The correction to $2J_{\perp}$ is always negative (that is, the interbath hopping is suppressed, as it usually happens for polarons [2] and spin-boson models [25]), and it is quite small in the low-momentum, weak coupling regime that we considered. However, notice that the expressions for these renormalized quantities are nonanalytic for $J_{\perp} = 0$.

The quantity $2\gamma_p$ is the width of the odd mode, and is proportional to J_{\perp} at small interbath hopping while saturating at a maximum value for large J_{\perp} . However, the latter behavior has to be taken with caution, because in the large- J_{\perp} regime bosonization is not applicable. See the end of Sec. IV.

APPENDIX C: SECOND-ORDER TERMS

In this Appendix we give details on the determination of the second-order correction to the state evolution, Eq. (49). In order to implement the perturbative procedure, we have to find the various second-order contributions among all terms in the expansion, which we will indicate with $(\dots)^{(2)}$,

$$(\Delta\mathcal{H}(t)|p\mu, \omega)^{(2)} = e^{2i\mu J_{\perp} t} \langle V(t) | p\bar{\mu}, \omega \rangle + \sum_{q\sigma, q'\sigma'} \frac{qq'}{2M} \frac{W_{q\sigma} W_{q'\sigma'}}{4L} \chi_t^*(\Omega_{q\sigma}) \chi_t^*(\Omega_{q'\sigma'}) b_{q\sigma}^{\dagger} b_{q'\sigma'}^{\dagger} |p\mu, \omega\rangle, \quad (\text{C1a})$$

$$\begin{aligned} (\Delta\mathcal{H}(t)|\phi_{p\mu}^{(1)}(t))^{(2)} &= \Delta E_{p\mu}^{(2)} |p\mu, \omega\rangle + \sum_{q\sigma, q'\sigma'} \sigma \sigma' \frac{W_{q\sigma} W_{q'\sigma'}}{4L} \chi_t^*(\Omega_{q\sigma}^{+\mu}(p)) e^{i\Omega_{q'\sigma'}^{-\mu} t} b_{q\sigma}^{\dagger} b_{q'\sigma'}^{\dagger} |p\mu, \omega\rangle \\ &+ \sum_{q\sigma, q'\sigma'} \sigma \frac{qq'}{M} \frac{W_{q\sigma} W_{q'\sigma'}}{4L} \chi_t^*(\Omega_{q\sigma}^{+\mu}(p)) \chi_t^*(\Omega_{q'\sigma'}(p)) b_{q\sigma}^{\dagger} b_{q'\sigma'}^{\dagger} |p\mu, \omega\rangle, \end{aligned} \quad (\text{C1b})$$

$$(\Delta\mathcal{H}(t)|\delta_2\phi_{p\mu}^{(2)}(t))^{(2)} = \frac{P_b^2}{2M} |\phi_{p\mu}^{(2)}(t)\rangle = \sum_v \sum_{q\sigma, q'\sigma'} \frac{qq'}{M} A_{q\sigma, q'\sigma'}^{\mu\nu}(p, t) b_{q\sigma}^{\dagger} b_{q'\sigma'}^{\dagger} |pv, \omega\rangle. \quad (\text{C1c})$$

The first term on the right-hand side (rhs) of Eq. (C1a) yields what we called $|\delta_1\phi_{p\mu}^{(2)}(t)\rangle$ [see Eq. (48)]. The first term on the rhs of Eq. (C1b) would give rise to secular behavior, and it is canceled by the perturbative procedure [see Eq. (34)]. All the remaining terms contain two phonon creation operators, and thus contribute to what we called $|\delta_2\phi_{p\mu}^{(2)}(t)\rangle$. The latter is determined by an equation of the form

$$\begin{aligned} i \frac{d}{dt} |\delta_2\phi_{p\mu}^{(2)}(t)\rangle &= \sum_v \sum_{q\sigma, q'\sigma'} i \frac{d}{dt} A_{q\sigma, q'\sigma'}^{\mu\nu}(p, t) b_{q\sigma}^{\dagger} b_{q'\sigma'}^{\dagger} |pv, \omega\rangle \\ &= \sum_v \sum_{q\sigma, q'\sigma'} \left(\frac{qq'}{M} A_{q\sigma, q'\sigma'}^{\mu\nu}(p, t) \right. \\ &\quad \left. + S_{q\sigma, q'\sigma'}^{\mu\nu}(p, t) \right) b_{q\sigma}^{\dagger} b_{q'\sigma'}^{\dagger} |pv, \omega\rangle, \end{aligned} \quad (\text{C2})$$

where we put all terms in Eqs. (C1a) and (C1b) involving two creation operators into the matrix $S_{q\sigma, q'\sigma'}^{\mu\nu}(p, t)$. Multiplying the above equation by $\langle pv, \omega | b_{q'\sigma'} b_{q\sigma}$ to the left, and taking into account that $A_{q\sigma, q'\sigma'}^{\mu\nu}(p, t)$ is symmetric under exchange of $q\sigma$ and $q'\sigma'$, while $S_{q\sigma, q'\sigma'}^{\mu\nu}(p, t)$ is not,

we find

$$\begin{aligned} i \frac{d}{dt} A_{q\sigma, q'\sigma'}^{\mu\nu}(p, t) &= \frac{qq'}{M} A_{q\sigma, q'\sigma'}^{\mu\nu}(p, t) \\ &+ \frac{1}{2} (S_{q\sigma, q'\sigma'}^{\mu\nu}(p, t) + S_{q'\sigma', q\sigma}^{\mu\nu}(p, t)), \end{aligned} \quad (\text{C3})$$

which is readily integrated,

$$\begin{aligned} A_{q\sigma, q'\sigma'}^{\mu\nu}(p, t) &= -ie^{-i\frac{qq'}{M}t} \int_0^t dt' e^{i\frac{qq'}{M}t'} \\ &\times \frac{1}{2} (S_{q\sigma, q'\sigma'}^{\mu\nu}(p, t') + S_{q'\sigma', q\sigma}^{\mu\nu}(p, t')). \end{aligned} \quad (\text{C4})$$

Performing the integral, we arrive at the results quoted in the main text, Eqs. (50) and (51).

APPENDIX D: COMPARISON WITH THE LINKED-CLUSTER EXPANSION

In a previous paper [15], we calculated the Green's function (or fidelity, if $\sigma' = \sigma$)

$$G_{\sigma'\sigma}(p, t) = -i \langle 0, \omega | d_{p\sigma'} e^{-i\mathcal{H}t} d_{p\sigma}^{\dagger} | 0, \omega \rangle \quad (\text{D1})$$

using the linked cluster expansion (LCE) perturbative technique. In the symmetric-bath case, it was calculated to be

$$G_{\sigma'\sigma}^{\text{LCE}}(p, t) = -\frac{i}{2} e^{F(0,t)} (e^{-i\lambda_{p\sigma}t + F(-J_{\perp},t)} + \sigma\sigma' e^{-i\lambda_{p\sigma}t + F(J_{\perp},t)}), \quad (\text{D2})$$

where

$$F(J, t) \equiv \int_0^{+\infty} d\varepsilon \frac{1 - (\varepsilon - 2J)t - e^{-i(\varepsilon - 2J)t}}{(\varepsilon - 2J)^2} R^S(\varepsilon). \quad (\text{D3})$$

It is easy to see that the perturbative approach that we developed in the present article is capable of reproducing the same result. In general

$$G_{\sigma\sigma}(p, t) = -i\theta(t) \langle p\sigma | e^{-i\mathcal{H}t} | p\sigma \rangle = \frac{1}{2} \sum_{\mu} [G_{\mu\mu}(p, t) + \sigma G_{\bar{\mu}\mu}(p, t)], \quad (\text{D4a})$$

$$G_{\bar{\sigma}\sigma}(p, t) = -i\theta(t) \langle p\bar{\sigma} | e^{-i\mathcal{H}t} | p\sigma \rangle = -\frac{1}{2} \sum_{\mu} [G_{\mu\mu}(p, t) - \sigma G_{\bar{\mu}\mu}(p, t)], \quad (\text{D4b})$$

where

$$G_{\mu\nu}(p, t) \equiv -i\theta(t) \langle p\mu, \omega | e^{-i\mathcal{H}t} | p\nu, \omega \rangle. \quad (\text{D5})$$

In our perturbative approximation $e^{-i\mathcal{H}t} | p\mu, \omega \rangle \approx |\psi_{p\mu}\rangle$ [Eq. (53) or (54)], hence

$$G_{\mu\mu}(p, t) = -ia_{p\mu}(t) e^{-i\lambda_{p\mu}t} \langle \omega | \omega_p(t) \rangle, \quad (\text{D6a})$$

$$G_{\bar{\mu}\mu}(p, t) = -ia_{p\mu}(t) e^{-i\lambda_{p\bar{\mu}}t} \langle \omega | \omega_p(t) \rangle \tilde{B}_{p\mu}(t). \quad (\text{D6b})$$

One can readily identify $a_{p\mu}(t) \equiv e^{F(-\mu J_{\perp}, t)}$, and calculate that $\langle \omega | \omega_p(t) \rangle = e^{F(0,t)}$. Therefore, in the symmetric case when $\tilde{B}_{p\mu}(t) = 0$, we recover exactly Eq. (D2).

The comparison with the LCE Green's function in the asymmetric case is less clear, because both in the LCE and in the perturbative technique of this paper the corresponding function depends explicitly on the cutoff Λ .

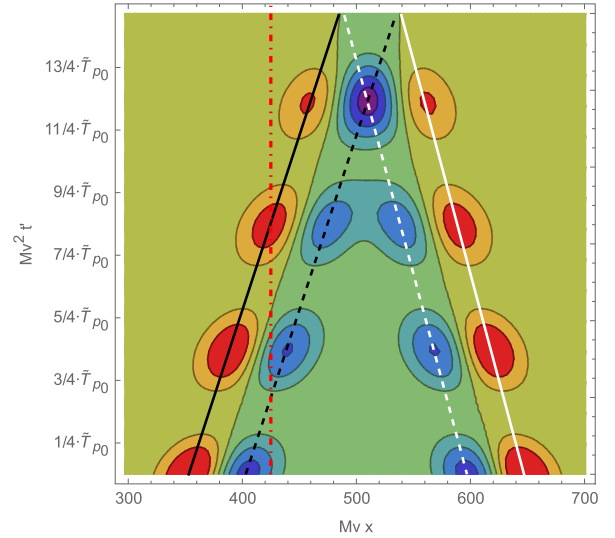
APPENDIX E: BATH DENSITY EVOLUTION FROM LINEAR RESPONSE

In this Appendix, we use Eq. (25) to obtain a qualitative and quantitative understanding of the observed behavior of the time evolution of the bath density profiles.

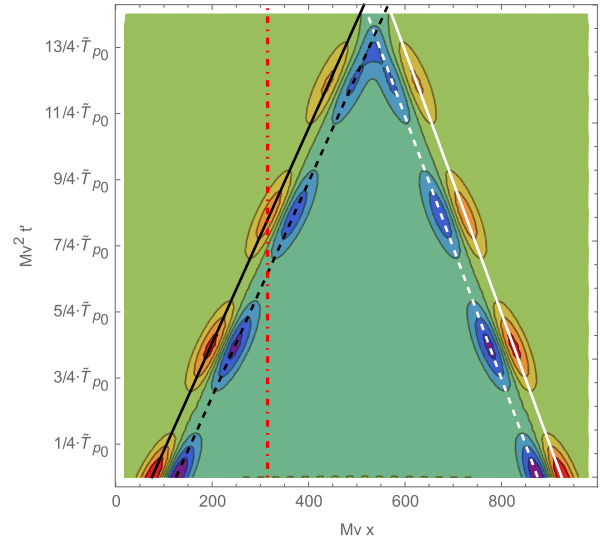
We repeat the equation here, for clarity,

$$\langle \rho_{\sigma}(x) \rangle_t = \frac{g_{\sigma} K_{\sigma}}{2\pi} \int_0^t dt' \left[\partial_{x'} \langle N_{\sigma}(x') \rangle_{t'} \Big|_{x'=x+v_{\sigma}(t-t')} - \partial_{x'} \langle N_{\sigma}(x') \rangle_{t'} \Big|_{x'=x-v_{\sigma}(t-t')} \right].$$

In Fig. 14 we show the integrand of Eq. (25), using a numerical lattice derivative of the interacting impurity density we computed in Sec. V A for $g^2 K = 0.5v^2$, in the \uparrow bath and for two different values of the interbath hopping. The wave packets are composed of $N_p = 32$ momenta, and are initially Gaussian with standard deviation $\delta p = 0.02Mv$ in momentum, which translates to a spatial width of $\delta x \approx 1/(2\delta p) = 25(Mv)^{-1}$. In the notation of Eq. (25), the time t at which we want to calculate the bath density is fixed in each plot



(a) $J_{\perp} = 0.1 M v^2$



(b) $J_{\perp} = 0.03 M v^2$

FIG. 14. Contour plot of the integrand of Eq. (25), computed with the impurity density obtained numerically. Warm colors correspond to positive values, while cold colors indicate negative values (the color-coded legends have been omitted since the quantitative values of the functions are irrelevant at the qualitative level of the discussion). The coupling is $g^2 K = 0.5v^2$ (symmetric baths), with a Gaussian wave packet composed of $N_p = 32$ momenta with standard deviation $\delta p = 0.02Mv$. Time is measured in units of the interacting density oscillation period $\tilde{T}_{p_0} = \pi/\tilde{J}_{\perp,p_0}$ (the absolute timescales of the two plots are therefore different). For the meaning of the various lines, see the text.

(and coincides with the maximum time shown), while the horizontal and vertical axes of the figures run along the desired position x and the integration time t' , respectively. Therefore, the bath density at a given position is obtained by integration along a vertical line, as the red dotted-dashed lines shown as examples. To highlight the periodicity of the oscillations, we measure time in the renormalized period of density oscillations, $\tilde{T}_{p_0} \equiv \pi/\tilde{J}_{\perp,p_0}$. As the impurity density

is essentially a Gaussian, its derivative has both a positive and a negative part, depicted in warm and cold colors, respectively, and this two-lobe structure is repeated along the lines $t' = t + (x - x_0 - p_0 t/M)/v_{-\sigma}$ and $t' = t + (x - x_0 - p_0 t/M)/v_{+\sigma}$, as dictated by the causality structure of Eq. (25) (we are ignoring the small slowing down of the impurity momentum) and by the periodic oscillations from one bath to the other. Recall that $v_{\pm\sigma} \equiv v_{\sigma} \pm p_0/M$. The four tilted lines show the approximate loci of the maxima and minima: $t' = t + (x - x_0 - p_0 t/M \pm \delta x)/v_{-\sigma}$ for the black lines and $t' = t - (x - x_0 - p_0 t/M \pm \delta x)/v_{-\sigma}$ for the white ones. Notice that we are neglecting the increase in width of the wave packet during its dynamics. It can be seen in the figures that it does not seem to play a relevant role, so we take δx to be the initial standard deviation.

If we compare the bath densities in Fig. 8(b), we see that Fig. 14(a) corresponds to a situation in which there are no ripples, while Fig. 14(b) gives rise to ripples. Now it is easy to understand how this situation emerges from Eq. (25). Let us take the position corresponding to the red line in Fig. 14(a). We see that during the time integration we encounter a positive contribution and part of two negative lobes belonging to the previous two impurity oscillations. The results will thus be close to zero. On the other hand, the integration path in Fig. 14(b) only encounters a positive lobe, and therefore it will give rise to the positive part of a ripple. If we change position, the same situation occurs: For $J_{\perp} = 0.1Mv^2$, any vertical line will always cross regions of both signs, with the result that it will always close to zero, while for $J_{\perp} = 0.03Mv^2$ it will alternatively cross positive and negative regions, resulting in oscillations of the density, i.e., the ripples. Thus, we see that the ripples emerge from an interference effect between subsequent oscillations of the impurity. The extent of this interference is regulated the interplay between the periodic impurity oscillations, the sound speed and the width of the wave packet. We can make a quantitative estimate of the parameters needed for a destructive interference: it happens whenever the oscillation period is such that the position of a positive lobe overlaps with the position of the negative lobe of the previous oscillation. With the help of Fig. 14, this translates to

$$v_{\pm\sigma} \tilde{T}_{p_0} \lesssim 2\delta x, \quad (\text{E1})$$

which directly leads to Eqs. (81) and (82) in the main text.

The only regions that are exempted from this interference mechanism are the farthest positions reachable by causality, $|x - x_0| \approx vt$, and the ones around the center $x \approx x_0 + p_0 t/M$, which are easily identified with the wave fronts and the central depletion of the bath density, respectively. Indeed, from Fig. 14 we can see that for $|x - x_0| \approx vt$ the time integral intersects only positive lobes, while around $x = x_0 + p_0 t/M$ there is a region with only negative contributions. Therefore, we obtain the features we observed in Sec. VID, namely that the wave fronts are always positive, while the depletion is always negative. These arguments also show that the wave fronts are images of the impurity density at the initial time, whereas the depletion is sensitive only to the density in the near past. In the main text, we claimed that the wave fronts and the central dip were images of the impurity density. This claim would be exactly true if the density evolution were given sim-

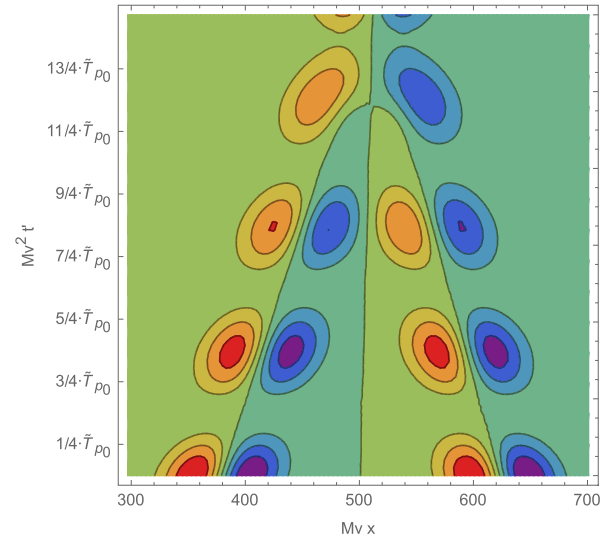


FIG. 15. Contour plot of the integrand of Eq. (E3), yielding the bath momentum density. The parameters are the same as Fig. 14(a) (in particular, $J_{\perp} = 0.1Mv^2$).

ply by a translation: $\langle d_{\sigma}^{\dagger}(x')d_{\sigma}(x') \rangle_t = N_0(x - x_0 - p_0 t/M)$, where $N_0(x - x_0)$ is the initial profile shape,

$$\begin{aligned} \langle \rho_{\sigma}(x, t) \rangle_t &= \frac{g_{\sigma} K_{\sigma}}{2\pi} \left[\frac{1}{v_{+\sigma}} N_0(x - x_0 + vt) \right. \\ &\quad - \left. \left(\frac{1}{v_{+\sigma}} - \frac{1}{v_{-\sigma}} \right) N_0(x - x_0 + p_0 t/M) \right. \\ &\quad \left. + \frac{1}{v_{-\sigma}} N_0(x - x_0 - vt) \right]. \end{aligned}$$

We can easily recognize the first and the last terms as the two counter-propagating wave fronts, which are translated images of the wave packet, and a negative depletion that follows the impurity. We also see that the heights of the wave fronts are different from each other, with the backward being shorter than the forward one, the difference being larger the faster is the impurity. The equation above is valid only in a highly idealized situation, in which there is only one bath ($J_{\perp} = 0$) and the wave packet does not spread. In our situation, both hypotheses are false, but we can guess that the most relevant phenomena are caused by the retardation effects given by the density oscillations [44]. For instance, the ratio of the wave fronts heights of the bath density we computed numerically tends to $v_{+\sigma}/v_{-\sigma}$ at long times.

As a final remark, we point out that the same arguments given above can be repeated for the bath momentum density, which is connected to the impurity density through an equation analogous to (22), with the response function

$$\chi_{\sigma}^{\Pi\rho}(x, t) = -\theta(t) \frac{1}{2\pi} [\delta'_{\alpha}(x + v_{\sigma} t) + \delta'_{\alpha}(x - v_{\sigma} t)]. \quad (\text{E2})$$

We can see that we obtain the analogous of Eq. (25), but with the two translated density gradients added to each other

instead of being subtracted,

$$\begin{aligned} \langle \Pi_\sigma(x) \rangle_t = & -\frac{g_\sigma}{2\pi} \int_0^t dt' \left[\partial_{x'} \langle N_\sigma(x') \rangle_{t'} \Big|_{x'=x+v_\sigma(t-t')} \right. \\ & \left. + \partial_{x'} \langle N_\sigma(x') \rangle_{t'} \Big|_{x'=x-v_\sigma(t-t')} \right]. \end{aligned} \quad (\text{E3})$$

- [1] J. Kondo, Resistance minimum in dilute magnetic alloys, *Prog. Theor. Phys.* **32**, 37 (1964).
- [2] G. D. Mahan, *Many-Particle Physics*, 2nd ed. (Plenum Press, New York, 1993)
- [3] A. C. Hewson, *The Kondo Problem to Heavy Fermions*, Cambridge Studies in Magnetism (Cambridge University Press, Cambridge, 1993).
- [4] L. Landau, On the motion of electrons in a crystal lattice, *Phys. Z. Sowjet.* **3**, 664 (1933).
- [5] L. D. Landau and S. I. Pekar, Effective mass of a polaron, *Zh. Eksp. Teor. Fiz.* **18**, 419 (1948).
- [6] J. T. L. Devreese, Fröhlich polarons. Lecture course including detailed theoretical derivations, [arXiv:1012.4576v6](https://arxiv.org/abs/1012.4576v6).
- [7] M. Lewenstein, A. Sanpera, and V. Ahufinger, *Ultracold Atoms in Optical Lattices: Simulating Quantum Many-Body Systems*, 1st ed. (Oxford University Press, Oxford, 2012).
- [8] I. Bloch, J. Dalibard, and W. Zwerger, Many-body physics with ultracold gases, *Rev. Mod. Phys.* **80**, 885 (2008).
- [9] C. J. Pethick and H. Smith, *Bose–Einstein Condensation in Dilute Gases*, 2nd ed. (Cambridge University Press, Cambridge, 2008).
- [10] F. Grusdt and E. Demler, New theoretical approaches to Bose polarons, [arXiv:1510.04934](https://arxiv.org/abs/1510.04934).
- [11] P. Massignan, M. Zaccanti, and G. M. Bruun, Polarons, dressed molecules and itinerant ferromagnetism in ultracold Fermi gases, *Rep. Prog. Phys.* **77**, 034401 (2014).
- [12] F. Meinert, M. Knap, E. Kirilov, K. Jag-Lauber, M. B. Zvonarev, E. Demler, and H.-C. Nägerl, Bloch oscillations in the absence of a lattice, *Science* **356**, 945 (2017).
- [13] J. Catani, G. Lamporesi, D. Naik, M. Gring, M. Inguscio, F. Minardi, A. Kantian, and T. Giamarchi, Quantum dynamics of impurities in a one-dimensional Bose gas, *Phys. Rev. A* **85**, 023623 (2012).
- [14] S. Palzer, C. Zipkes, C. Sias, and M. Köhl, Quantum Transport through a Tonks-Girardeau Gas, *Phys. Rev. Lett.* **103**, 150601 (2009).
- [15] M. Stefanini, M. Capone, and A. Silva, Motion of an impurity in a two-leg ladder, *Phys. Rev. B* **103**, 094310 (2021).
- [16] P. Zubko, S. Gariglio, M. Gabay, P. Ghosez, and J.-M. Triscone, Interface physics in complex oxide heterostructures, *Annu. Rev. Condens. Matter Phys.* **2**, 141 (2011).
- [17] H. Y. Hwang, Y. Iwasa, M. Kawasaki, B. Keimer, N. Nagaosa, and Y. Tokura, Emergent phenomena at oxide interfaces, *Nat. Mater.* **11**, 103 (2012).
- [18] C. M. Kropf, A. Valli, P. Franceschini, G. L. Celardo, M. Capone, C. Giannetti, and F. Borgonovi, Towards high-temperature coherence-enhanced transport in heterostructures of a few atomic layers, *Phys. Rev. B* **100**, 035126 (2019).
- [19] The statistics of the particles forming the baths will turn out to be irrelevant within our approximations. As there is only one impurity in the system, its statistics is rigorously irrelevant, but to fix the notation we choose to work with a fermionic impurity.
- [20] T. Giamarchi, *Quantum Physics in One Dimension*, 1st ed. (Clarendon Press, Oxford, 2003).
- [21] A. O. Gogolin, A. A. Nersisyan, and A. M. Tsvelik, *Bosonization and Strongly Correlated Systems* (Cambridge University Press, Cambridge, 1998).
- [22] Throughout this paper, we use units in which $\hbar = 1$.
- [23] T. D. Lee, F. E. Low, and D. Pines, The motion of slow electrons in a polar crystal, *Phys. Rev.* **90**, 297 (1953).
- [24] In pbc the position operator is of course ill-defined. However, the LLP operator is perfectly defined because P_b is quantized in multiples of $2\pi/L$.
- [25] A. J. Leggett, S. Chakravarty, A. T. Dorsey, M. P. A. Fisher, A. Garg, and W. Zwerger, Dynamics of the dissipative two-state system, *Rev. Mod. Phys.* **59**, 1 (1987).
- [26] We are using $W_{q\sigma} = W_{-q\sigma}$ to change the sign of the momentum label of the annihilation operator.
- [27] W. T. Langhoff, S. T. Epstein, and M. Karplus, Aspects of time-dependent perturbation theory, *Rev. Mod. Phys.* **44**, 602 (1972).
- [28] C. M. Bender and S. A. Orsag, *Advanced Mathematical Methods for Scientists and Engineers I*, 1st ed. (Springer, New York, 1999).
- [29] A. Auerbach, *Interacting Electrons and Quantum Magnetism*, 1st ed. (Springer-Verlag, Berlin, 1994).
- [30] Notice that $\langle V(t) \rangle$ is nonvanishing only if the baths are asymmetric, in which case it is logarithmically divergent in the TLL cutoff.
- [31] F. Chevy, Universal phase diagram of a strongly interacting Fermi gas with unbalanced spin populations, *Phys. Rev. A* **74**, 063628 (2006).
- [32] Notice that we are setting explicitly $\langle \Psi_t | \Psi_t \rangle \equiv 1$. However, this is true only for short times with respect to $\min_p (2\gamma_p)^{-1}$, because of the perturbative normalization. If we were to take this into account, we would have $\sum_\sigma \langle n_\sigma \rangle_t$ decreasing from 1 in time.
- [33] If the physical meaning of $\rho_\sigma(x)$ is obvious, it may be less so for the momentum density $\Pi_\sigma(x)$. The equation of motion for the density (i.e., the continuity equation) shows that, within our long-wavelength approximation, $\Pi_\sigma(x)$ is proportional to the particle current: $j_\sigma(x) = v_\sigma K_\sigma \Pi_\sigma(x)$.
- [34] More specifically, we define $n_{p_0} \in \mathbb{Z}$ such that $p_0 = 2\pi/L n_{p_0}$, then we take $p_n = 2\pi/L(n_{p_0} + n)$ where $n = -N_p/2 + 1, \dots, N_p/2$ when N_p is even, and $n = -(N_p - 1)/2, \dots, (N_p - 1)/2$ when N_p is odd.
- [35] As we did with $\langle n_\sigma \rangle_t$, writing it as $1/2 + \sigma \langle \sigma_3 \rangle_t / 2$, we take $\langle P \rangle_t = \langle P \rangle_{t=0} = p_0$, i.e., we ignore the effect of the loss of normalization on the conserved total momentum.
- [36] This transient in the momentum evolution may be linked to a dimensional crossover, which is also shown by the Green's function [15].
- [37] M. Schechter, D. Gangardt, and A. Kamenev, Dynamics and Bloch oscillations of mobile impurities in one-dimensional quantum liquids, *Ann. Phys.* **327**, 639 (2012).

- [38] We point out that the existence of the band degree of freedom is crucial for the present arguments: energy and momentum conservation implies that a purely 1D impurity (i.e., $J_{\perp} = 0$) cannot emit real phonons.
- [39] This is in accord with the observation that in the interacting case $\langle n_{\sigma} \rangle_t$ never goes back to 0 or 1 for $t > 0$.
- [40] The relation $\delta x = 1/(2\delta p)$ is only approximately valid for our discrete Gaussian wave packet.
- [41] For instance, notice that the “snapshots” in Fig. 10 cover an area in (r, R) space, which is quite smaller than the maximal rectangle $[-L, L] \times [0, L]$ beyond which the periodicity of the boundary conditions sets in.
- [42] A. Kantian, U. Schollwöck, and T. Giamarchi, Competing Regimes of Motion of 1D Mobile Impurities, *Phys. Rev. Lett.* **113**, 070601 (2014).
- [43] DLMF, NIST Digital Library of Mathematical Functions, <http://dlmf.nist.gov/>, Release 1.0.25 of 2019-12-15, F. W. J. Olver, A. B. Olde Daalhuis, D. W. Lozier, B. I. Schneider, R. F. Boisvert, C. W. Clark, B. R. Miller, B. V. Saunders, H. S. Cohl, and M. A. McClain, eds.
- [44] Indeed, it is possible to obtain an analytic expression of the bath density if we take $\langle d_{\sigma}^{\dagger}(x')d_{\sigma}(x') \rangle_t = N_0(x - x_0 - p_0 t/M)(\cos J_{\perp} t')^2$, that is, if we again discard the wave packet spreading. In the solution, we can still recognize the presence of the wave fronts and the depletion.